11-1-2014

Comparing Near-Regional and Local Measurements of Infrasound from Mount Erebus, Antarctica: Implications for Monitoring

A. L. Dabrowa
University of Bristol

D. N. Green
AWE Blacknest

J. B. Johnson
Boise State University

J. C. Phillips
University of Bristol

A. C. Rust
University of Bristol

Publication Information

Dabrowa, A.L.; Green, D.N.; Johnson, J.B.; Phillips, J.C.; and Rust, A.C. (2014). "Comparing Near-Regional and Local Measurements of Infrasound from Mount Erebus, Antarctica: Implications for Monitoring". *Journal of Volcanology and Geothermal Research*, 288, pp. 46-61. doi: 10.1016/j.jvolgeores.2014.10.001

Comparing near-regional and local measurements of infrasound from Mount Erebus, Antarctica: Implications for monitoring

A. L. Dabrowa*[a], D. N. Green[b], J. B. Johnson[c], J. C. Phillips[a], A. C. Rust[a].

[a]School of Earth Sciences, University of Bristol, Wills Memorial Building, Queen's Road, Bristol, BS8 1RJ, UK.

[b]AWE Blacknest, Reading, RG7 4RS, UK.

[c]Dept. Of Geosciences, Boise State University, 1910 University Drive, Boise, Idaho, 83725-1535, US.

*Corresponding author. School of Earth Sciences, University of Bristol, Wills Memorial Building, Queen's Road, Bristol, BS8 1RJ, UK. Tel.: +44 117 9545400; fax: +44 117 9253385. Email address: amy.dabrowa@bristol.ac.uk.

Abstract

Local (100s of meters from vent) monitoring of volcanic infrasound is a common tool at volcanoes characterized by frequent low-magnitude eruptions, but it is generally not safe or practical to have sensors so close to the vent during more intense eruptions. To investigate the potential and limitations of monitoring at near-regional ranges (10s of km) we studied infrasound detection and propagation at Mount Erebus, Antarctica. This site has both a good local monitoring network and an additional International Monitoring System infrasound array, IS55, located 25 km away. We compared data recorded at IS55 with a set of 117 known Strombolian events that were recorded with the local network in January 2006. 75% of these events were identified at IS55 by an analyst looking for a pressure transient coincident with an F-statistic detection, which identifies coherent infrasound signals. With the data from January 2006, we developed and calibrated an automated signal-detection algorithm based on threshold values of both the F-statistic and the correlation coefficient. Application of the algorithm across IS55 data for all of 2006 identified infrasonic signals expected to be Strombolian explosions, and proved reliable for indicating trends in eruption frequency. However, detectability at IS55 of known Strombolian events depended strongly on the local signal amplitude: 90% of events with local amplitudes > 25 Pa were identified at IS55, compared to only 26% of events with local amplitudes <25 Pa. Event detection was also affected by considerable variation in amplitude decay rates between the local and near-regional sensors. Amplitudes recorded at IS55 varied between 3% and 180% of the amplitude expected assuming hemispherical spreading, indicating that amplitudes recorded at near-regional ranges to Erebus are unreliable indicators of event magnitude. Comparing amplitude decay rates with locally collected

radiosonde data indicates a close relationship between recorded amplitude and lower atmosphere effective sound speed structure. At times of increased sound speed gradient, higher amplitude decay rates are observed, consistent with increased upward refraction of acoustic energy along the propagation path. This study indicates that whilst monitoring activity levels at near-regional ranges can be successful, variable amplitude decay rate means quantitative analysis of infrasound data for eruption intensity and magnitude is not advisable without consideration of local atmospheric sound speed structure.

Keywords

volcano monitoring

volcano infrasound

Mount Erebus

Infrasound propagation

1. Introduction

Infrasound is an effective tool for monitoring and studying explosive volcanic eruptions from distances of hundreds to thousands of km (Dabrowa et al., 2011, Matoza et al., 2011). However, long-distance acoustic propagation through the inhomogenous atmosphere complicates quantitative inversions of the data for eruption parameters, and acoustic propagation times restrict the timeliness of eruption warnings for local populations. Ideally, monitoring distances should be shorter so that warnings are more timely, signal to noise ratios (SNRs) are higher and propagation effects are reduced.

The range at which infrasound is recorded from volcanoes varies considerably depending on the type of volcanic activity and the purposes of the instrument deployment (see Fee and Matoza, 2013, for a review). The relatively low intensity of Strombolian explosions at volcanoes such as Stromboli, Erebus and Villarrica allows sensors to be safely deployed at distances of hundreds of meters (considered “local range” in this study) where the SNR is still high despite the relatively low amplitude of the infrasound generated by the eruptions (Johnson et al., 2008; Marchetti et al., 2009; Ripepe and Marchetti, 2002; Ripepe et al., 2010). It is necessary to monitor volcanoes that have more intense eruptions from a greater distance to reduce the risk of damage to equipment and personnel. The VEI 3 eruption of Augustine Volcano, Alaska, in 2006, destroyed much of the monitoring network, including all four seismic sensors located within 1.5 km of the vent and the only broadband seismic sensor, located 2.2 km from the vent (Petersen et al., 2006). This example

demonstrates the need, where possible, to monitor volcanoes from a range of distances, including instruments at distances which ensure a sufficiently intact network during times of heightened activity and greatest need. At even greater distances of hundreds to thousands of km, infrasound could also be an effective tool for monitoring remote volcanoes with no local coverage (Dabrowa et al., 2011; Matoza et al., 2011). However, if feasible it is favourable to be more proximal to reduce propagation effects and increase the signal-to-noise ratio.

A number of recent studies have focused on infrasound recordings made close to the eruption site and have highlighted the variety of propagation effects that influence infrasound recorded at ranges of a few km to tens of km. At some geographical locations the acoustic propagation is dominated by the temporal change in acoustic ducting, where infrasonic energy undergoes refraction from an increase in acoustic velocity at altitude before being returned to the ground surface. Propagation in such a waveguide has been commonly observed for signals generated at the Pu'u 'Ō'ō crater complex, Kilauea (e.g., Fee and Garces, 2007). In a study of the same system, Matoza et al. (2010) found that signal amplitudes at 12km from the vent vary by more than double those recorded at 2km from the vent, as the shallow waveguide formed by the nocturnal boundary layer waxes and wanes across a diurnal cycle. Lacanna et al. (2014) show the effect of tropospheric ducting out to 60km from Sakurajima volcano, Japan. In this study, incorporating measured tropospheric windspeed variations into numerical acoustic propagation models assists in predicting the strength of acoustic ducting, and the amplitudes of observed arrivals.

At other locations, tropospheric acoustic waveguides are not regularly present. In these situations, acoustic propagation is controlled by the strength of upward acoustic refraction generated by the decrease in acoustic speed with altitude. This acoustic speed decrease is a function of both the negative temperature gradients with increasing altitude, and the along-path wind speed. Matoza et al. (2009) show that for low-amplitude infrasound signals recorded 13 km from the active dome at Mt. St. Helens, USA, the signal strength and inter-event correlation depend on the wind speeds along the source-to-receiver path. Unlike the diurnal amplitude changes seen at Kilauea, the Mt St. Helens signal amplitudes vary on timescales associated with mesoscale meteorological variations. Signals recorded 8 km from the vent of Villarrica, Chile, are also dependent upon the strength of upward acoustic refraction (Johnson et al., 2012). Signals recorded over a five day period exhibit amplitudes that vary between 0.4 and 1.2 times that expected for a 1/r hemispherical amplitude decay. These studies suggest that without corrections for propagation effects, eruption parameter

estimation (e.g. vent overpressure, following Vergniolle et al., 2004) based on infrasound recorded at ranges greater than a few km will be subject to significant uncertainties.

Mount Erebus, Antarctica, has a number of features that make it an outstanding field location for the study of locally recorded infrasound over an extended time period (months to years). Activity at Mount Erebus is dominated by Strombolian explosions from the summit lava lake. These occur several times each day and produce relatively simple, highly repeatable infrasound signals (Rowe et al., 2000). Furthermore, Mount Erebus is a well studied volcano with a network of infrasound sensors within hundreds of meters of the vent (e.g. Jones et al., 2008; Johnson et al., 2008). In our study we compare data from the local network to waveforms recorded at an array, IS55, located 25km SSE of Mount Erebus, (a 'near-regional' distance from the vent, using the terminology of Fee and Matoza, 2013). This has allowed us to quantify the effect of tropospheric infrasound propagation on the recorded signal characteristics.

IS55 is an eight element, 1.9 km aperture, microbarometer array that has been installed at Windless Bight, on the Ross Ice Shelf as part of the verification measures for the Comprehensive Nuclear-Test-Ban Treaty (e.g., Christie et al., 2010). The array was designed and deployed to record signals from atmospheric nuclear explosions with the passband of interest ranging from around 0.1 Hz to 10 Hz. The array aperture is optimal for detecting signals dominated by power at approximately 0.3 Hz. Although eruptions at Mount Erebus generate infrasound that is dominated by higher frequencies, with peak energies generally around 2 Hz (Johnson et al., 2008), this activity is regularly detectable in data from IS55 (Dabrowa et al., 2011).

The IS55 dataset could be useful for Erebus researchers even though the 25 km source-array distance is much greater than optimal for monitoring the relatively low amplitude infrasound produced by Strombolian activity. For example, the infrasound station IS55 has been in operation since August 2003 and as part of certification an IMS station is required to be operational for at least 98% of the time (Christie et al., 2010). In contrast, much of the instrumentation deployed locally on Erebus operates from solar panels and until at least the mid 2000s infrasonic sensors suffered from major gaps in data output in the austral winter (Jones et al., 2008). Infrasound data recorded at IS55 could therefore provide a more continuous record of the level of activity than the summit instrumentation.

In this paper we assess the detectability of infrasound generated at Erebus and compare the signals recorded at IS55 to those recorded at the vent. This provides insights into the way in which volcanic infrasound data recorded at near-regional ranges could be used for volcano research and monitoring. We develop a new methodology for automatically detecting infrasound from volcanic activity, exploiting and combining techniques commonly used in both local volcano monitoring scenarios and the processing of array data. Lastly, we assess how the automated event detection lists compiled using data recorded at IMS stations and published by the Comprehensive Nuclear-Test-Ban Treaty Organisation (CTBTO) might be used by volcano researchers.

2. Previous studies at Mount Erebus

Mount Erebus is a volcano on Ross Island, with a summit altitude of 3794 m. It is Antarctica's most active volcano, exhibiting regular activity since its discovery in 1841 (Oppenheimer and Kyle, 2008). Due to its continuous activity and its location close to McMurdo base (Figure 1, Figure 2) it has been the subject of detailed research since the 1970s. A lava lake referred to as Ray Lake has been present in the summit crater, passively degassing and actively convecting since at least 1972 when more regular monitoring of the volcano commenced (Sweeney et al., 2008). This lava lake is the source of the regular Strombolian explosions which characterise activity at Erebus. From 1972 to 2007 there were typically 2 to 6 explosions per day (Jones et al., 2008); however, the occurrence of up to 900 Strombolian explosions in a single day has been reported (Rowe et al., 2000). Notable exceptions to usual behaviour include heightened activity during late 1984 and late 2005 to at least April 2006 (including the period covered in this study) and decreased activity levels between August 2002 and January 2004.

The Mount Erebus Volcano Observatory (MEVO) was formed in 1992. Equipment installed initially included a 6-station telemetered seismic network and in 1996 the first permanent infrasonic microphone was co-located with one of the seismic stations (Rowe et al., 2000), although infrasound studies at Erebus began much earlier (e.g. Dibble, 1989). By 2005 the infrasound network had expanded to include 7 sensors at 5 separate locations between 320 and 820 m from Ray Lake. Additional monitoring at Erebus operated by MEVO includes video recording, infrared sensors, GPS and tiltmeters (Jones et al., 2008), supplemented by additional monitoring during temporary field campaigns, including COSPEC and DOAS (Sweeney et al., 2008), FTIR and thermal camera (Oppenheimer et al., 2009) and doppler radar (Gerst et al., 2008).

Infrasonic waveforms produced by Strombolian explosions in Ray Lake are generally short in duration (2-3 seconds for the high amplitude onset of the waveform) and comprise a high amplitude peak and trough followed by a coda of varied length and amplitude (Rowe et al. 2000; Figure 5). The frequency characteristics of waveforms generated by Strombolian explosions are consistent across a wide range of amplitudes (Rowe et al., 2000), with peak energy at approximately 2 Hz (Johnson et al., 2008). Though Strombolian explosions are commonly modelled as monopole sound sources, Johnson et al. (2008) also successfully modelled infrasound as a pure dipole source, motivated by the variation in amplitude observed with azimuthal location at sensors spaced around the lava lake. The deviation from vertical of the modelled dipole axis was found to be less than 20° in the majority of cases, and the authors suggest that a monopole source with an additional minor dipole component may prove to be a better fit to the data. Previous studies of Erebus acoustics have used infrasound to infer stratification of the magma column in the upper conduit (Rowe et al., 2000), detect and locate volcanic activity within the summit crater (Jones et al., 2008) and investigate the mechanisms of infrasound production during Strombolian explosions (Johnson et al., 2008).

The IMS infrasound array IS55 has been operating since 2003, however the array data have yet to be used within a detailed study of activity at Mount Erebus. Figure 1 shows all signals automatically detected by the CTBTO at IS55 over the period 1st January 2006 to 31st December 2006. Near-continuous detections from the direction of Erebus can be seen with a back-azimuth of approximately 336°. In addition, there are many high-frequency arrivals that exhibit similar back-azimuths, some of which can be attributed to the fracturing of local ice cliffs (Szuberla and Arnoult, 2011). Moreover, on telesonic scales, large numbers of detections are made with back-azimuths east and northeast of IS55 during the austral summer and from the west and north-west during the austral winter. These signals have propagated in efficient waveguides formed by high velocity stratospheric winds and illustrate the well-known influence of stratospheric wind direction on global infrasound propagation (e.g. Drob et al., 2003).

3. Data and methods

3.1 Data collection

IS55 consists of 8 Chaparral Model 5 microbarometers, each with a system of wind-noise reducing pipes connecting them to the atmosphere. Five outer sensors form a pentagon with an aperture of 1.9 km, and three additional sensors form an inner triangular array with an aperture of 173 m (Wilson et al., 2010; Figure 2; Table 1). Although the microbarometers have a frequency response which is flat to within 3 dB between 0.02 and 50 Hz (Christie and Campus, 2010), the attached wind

noise reduction system reduces the high-frequency response at IS55 (Fee and Gabrielson, pers. comm. 2014). The system response of IS55 has been measured using the method of Gabrielson (2013), and has been deconvolved from all pressure data used within this study. We have not attempted to account for minor response variations due to seasonal snow loading on the wind noise reduction system.

Also present at IS55 is a meteorological station with an anemometer located at 2 m height, a temperature sensor and an absolute barometer installed at 1 m height. Infrasound data are sampled at 20 Hz whilst temperature, wind direction and wind speed data are sampled at 1 Hz. Infrasound and meteorological data were acquired for this study for the whole of 2006. It is noted that IS55 is situated on the ice of Windless Bight, and therefore moves at approximately 65m/yr (Fee, pers. Comm. 2014). Therefore, within a year the distance between the summit of Erebus and the array can vary by up to 0.3% of the path length.

The full automated detection list compiled by the CTBTO for IS55 was obtained for the period 17th Jan 2004 to 31st December 2011. This list contains coherent infrasound signal detection parameters identified using the PMCC (Progressive Multi-Channel Correlation) algorithm used by the CTBTO (Cansi, 1995). These parameters include the signal arrival time, the backazimuth, the apparent velocity, and the central frequency of the detection passband. We note that the CTBTO employs a scheme to cluster detections across a number of passbands to provide a single broadband detection (see Brachet et al., 2010, for details).

IS55 data were compared to those recorded at three stations located around the summit crater of Erebus, 325-822 m from the centre of Ray Lake (SHK, RAY and E1S; Figure 2; Table 1) and collected by Jones et al. (2008) during a field campaign in early 2006. Data from SHK were used for much of the analysis in this paper (e.g. for timings of known Strombolian events and measurements of ambient noise levels at the vent) because it is the closest local station to the centre of Ray Lake. However, to limit effects of amplitude directionality, data from RAY are used for comparisons of local and IS55 amplitudes because RAY and IS55 have similar backazimuths to Ray Lake (see section 2 and Figure 2). The sensors at SHK, RAY and E1S are Honeywell model DC001NDR5 pressure transducers, which are reported to have a flat frequency response over the frequencies of interest in this study and a wide dynamic range with linear instrument response at pressures up to ± 250 Pa (Johnson et al., 2008). For further details on instrument deployment see Jones et al. (2008). The local sensor locations provided line-of-sight propagation paths from the lava lake (Johnson et al., 2008). Waveform data for a set of 117 Strombolian events in the Ray Lake, recorded at SHK, RAY

and E1S for January 2006 (excluding the 14th and 16th) were acquired in the form of filtered pressure timeseries of 108 second duration for each event. These data comprise a subset of the volcanic signals automatically detected by Jones et al. (2008) by calculating the cross correlation coefficient (C, described in section 3.3) between data recorded at the local sensors. These authors identified an event as occurring when C exceeded 0.3 across all three sensor pairs. This dataset of 117 Strombolian events will be referred to in this paper as "known Strombolian events". A timing discrepancy (known to be stable with time) of approximately -36 seconds exists in the local data supplied to us and therefore for this work 36 seconds have been deducted from the timings of all local data. Timings and amplitudes of the 117 known Strombolian events are given in Appendix A.

Table 1 Location data for stations SHK, RAY, E1S and IS55

Station name	Latitude	Longitude	Altitude (m)
SHK	-77.5261	167.1559	3774
RAY	-77.5286	167.1708	3766
E1S	-77.5305	167.1398	3659
IS55	-77.73	167.62	41

As detailed above and later in the paper, this study utilised a number of datasets consisting of both local and regionally recorded infrasound and lists of detected events compiled by different authors and methods. A summary of these are provided as a reference to the reader in Table 2 below.

Table 2 Summary of main datasets used in study

Data Type	Time period covered	Source of Data	How data are used in this study
Times of known Strombolian events at Erebus (detected proximally)	Jan to March 2006	Subset of those events originally detected by Jones et al. (2008)	Identifying infrasound signals detected at IS55 from known Strombolian events at Erebus and using these signals to create stacked waveform for automatic event detection (section 3.3).
Infrasound data recorded at the proximal stations	Data from 117 known Strombolian events from January 2006 (excluding events on the 14th and 16th)	Subset of those events originally detected by Jones et al. (2008)	Comparing amplitudes of signals recorded at IS55 with those at the proximal stations, calculating propagation times
Infrasound data recorded at IS55	Jan 1st to December 31st 2006	CTBTO	Comparing amplitudes of signals recorded at IS55 with those at the proximal stations, calculating propagation times; automatically detecting events over the whole of 2006; calculating background noise levels at IS55.
Lists of events detected by the CTBTO automatic detection algorithm	17th Jan 2004 to 31st December 2011	CTBTO	Comparing with event times detailed above to investigate detection of Strombolian events at Erebus by the CTBTO.
List of events detected automatically by Knox	2003 to 2011	Knox (2012)	Comparing to events automatically detected using our methods (section 3.3) and by the CTBTO

3.2 Data processing and manual identification of infrasonic signals at IS55

The measured sensor response was deconvolved from infrasound data recorded at each of the IS55 microbarometers to provide pressure timeseries with units of Pascals (Pa). The data was subsequently filtered and beamformed.

In a previous study of global volcanic infrasound detections (Dabrowa et al., 2011) it was found that infrasound produced by Strombolian explosions at Erebus were detectable above the ambient noise at IS55 at frequencies between 0.1 Hz and 4.45 Hz. Consequently, all infrasound data from IS55 were initially filtered using a Butterworth 2 pole causal filter with a pass band of 0.4 – 4 Hz. Though this filters out some of the signal energy it ensures that contamination of the signals with microbarom noise is avoided (dominant frequency ~0.2 Hz, Bowman et al., 2005) and improves

signal to noise ratios enabling easier identification of lower amplitude signals. The local data from known Strombolian events recorded at sensors SHK, RAY and E1S had been previously bandpass filtered between 0.25 Hz and 20 Hz using a Butterworth 2 pole acausal filter. Therefore, wherever IS55 data were compared to local data, the IS55 unfiltered array data were first re-filtered using a Butterworth 2 pole acausal filter with a high pass frequency of 0.25 Hz. Because the IS55 data are sampled at 20 Hz and therefore have a Nyquist frequency of 10 Hz, it should be noted that the signals recorded at IS55 will have reduced high frequency energy content compared to the local data. However, as the local data exhibit peak signal frequencies at ~2Hz, and the spectral content falls rapidly towards the noise floor above 5Hz (Figure 5) the effect is not expected to be significant.

Beamforming involves introducing time delays into the pressure records from each sensor in the array equal to the relative delay between sensors expected for a plane wavefront travelling across the array from a certain direction at a certain speed (e.g., Rost and Thomas, 2002). The pressure records are aligned so that the wavefront appears to arrive at all of the sensors simultaneously and pressure records from all sensors are summed and averaged to improve the signal to noise ratio (SNR). The optimal time delays for creating Erebus signal beams were identified using an F-detector that provides a measure of the across-array coherence for time-delayed traces. Theoretically calculated time delays for signals arriving across a swath of backazimuths and apparent velocities (the beamset) were applied to the array data for every signal, prior to the F-statistic (often referred to as the F-value) being calculated for consecutive 6s windows with 50% overlap:

$$= (\boldsymbol{N-1})\frac{\sum_{\boldsymbol{t=1}}^{\boldsymbol{M}} \breve{\boldsymbol{P}}(\boldsymbol{t})^{\boldsymbol{2}}}{\frac{\boldsymbol{1}}{\boldsymbol{N}}\sum_{\boldsymbol{t=1}}^{\boldsymbol{M}}\sum_{\boldsymbol{n=1}}^{\boldsymbol{N}} \boldsymbol{P_n}(\boldsymbol{t})^{\boldsymbol{2}} - \sum_{\boldsymbol{t=1}}^{\boldsymbol{M}} \breve{\boldsymbol{P}}(\boldsymbol{t})^{\boldsymbol{2}}} \quad [1]$$

where *N* is the number of sensors in the array, *M* is the number of samples in the data window, *P* is the pressure trace recorded on a sensor, $\breve{P}$ is the beamformed pressure trace and *t* is time. The F-statistic is a measure of the coherency of the sound wave passing across the array. It measures the power of the beam compared to the average over all individual sensors of the power of the individual sensor data minus the power of the beam (Blandford, 1974). Consequently as a coherent signal passes across the array and the correct time delays are applied, power on the beam increases and the difference between the beam and an individual pressure channel decreases resulting in an increased F-value. The optimum propagation parameters for a particular signal (backazimuth and apparent velocity) are chosen to be those that maximise the F-statistic.

In this study, an increase in the F-value coincident with an increase in pressure amplitude near the expected arrival time of an infrasonic signal from a known Strombolian event, allows a human analyst to confidently identify the signal as being associated with the Erebus event (Figure 3). For the set of known Strombolian eruptions at Erebus throughout January 2006, the optimal beams were centred on a backazimuth of 336.5+/-0.6° and an apparent velocity of 327+/-4m/s (uncertainties are given at the one standard deviation level). These results are consistent with those found from analysing the detection lists of the CTBTO (see Section 4.3).

Infrasonic signals from known Strombolian events recorded at both the local sensors and IS55 generally consisted of a high amplitude peak and trough in pressure, followed by a coda of varied length and amplitude. The maximum peak-to-peak (P2P) amplitude over the signal window and the time of the first peak in pressure of the signal recorded both at the local sensors and at IS55 were measured to allow comparison of the waveforms. For all known Strombolian events, mean values of meteorological parameters measured at IS55 (temperature, wind speed and wind direction) were also calculated for the 60 second period centred on the arrival time of the signal (estimated if an infrasonic signal from the event was not identified).

3.3. **Automatic detection of Strombolian events at Erebus**

If near-regional infrasound data are to be used effectively for volcano monitoring, volcanic events need to be detected automatically. In this paper we develop an automated detection method which combines techniques commonly used in local monitoring of volcanoes and in long-range infrasound detection. Infrasonic signals produced by those of the 117 known Strombolian events which were identified manually at IS55 (using methodology described in section 3.2) were used to characterise the infrasound signal expected from a Strombolian event at Erebus. The identified arrival times of these events at IS55 could also be used to assess the performance of the automated detection methods over the period of January 2006. This methodology was then expanded to automatically detect infrasound signals expected to be from Strombolian events at Erebus in data recorded at IS55 during the whole of 2006.

Firstly, an infrasound signal waveform which was typical of a Strombolian event at Erebus recorded at IS55 was created by stacking the signals from those known Strombolian events that were identified manually at IS55. These events included those from January 2006 and additional known Strombolian events from February and March 2006 reported in Johnson et al. (2008) and identified

at IS55 using the F-detector described in section 3.2. Next, continuous pressure data from IS55 (beamformed and filtered) were cross correlated with this typical waveform to identify periods where the infrasound signal recorded at IS55 was similar in shape to that typical of a Strombolian event at Erebus, resulting in a correlation coefficient, C, above a chosen threshold value (see below). The correlation coefficient (C) value and the previously discussed F-statistic (F) value can be used to automatically detect infrasound signals, either individually or in combination.

When coherent infrasound travelling as a plane wave arrives from the back-azimuth for which data are beamformed, the value of F will increase relative to the value associated with background noise. For simplicity, the automatic detectors only run the F-detector across one beam, not the entire beamset. The beam is chosen to align signals with a backazimuth of 336.5° and an apparent velocity of 327m/s. Given the tight distributions of propagation characteristics (backazimuths, apparent velocities) associated with Erebus events (see Section 3.2), reductions in F due to small deviations from the chosen beam have only a small effect on the detector. While the F detector assesses the level of signal coherence, the cross-correlation coefficient, C, calculated between the beam and the stacked waveform, assesses the similarity between the beam and signals known to have originated from Strombolian events at Erebus. C-detectors will be vulnerable to any changes in waveform including those derived from seasonal wind effects but we have not evaluated a sufficiently long time series to robustly test for seasonal effects.

Algorithms that trigger a detection each time the value of F and/or the value of C increases above a suitable threshold (Figure 3) were tested using a range of values of F and C to establish which method (F, C, or F and C in combination) and which thresholds were optimal. Threshold values of C were varied from 0.2 to 0.75 in increments of 0.05 and thresholds of F were varied from 2 to 30 in increments of 2 (Appendix B). The three methods are referred to as the F-detector, the C-detector and the FC-detector. All data points in the F and C variables that were above the chosen threshold value (F_{TH} or C_{TH}) and are also local maxima were identified and the corresponding times of these data points were recorded as detections using either the F- or C-detector. For the joint FC-detector, each of the F data points identified as above-threshold maxima were inspected to ascertain if there was also an identified C data point within 10 seconds. In this case, the time of the C data point was recorded as an FC-detection. A relatively long time window of 10 seconds length was used because the time resolution and windowing of the F-statistic can cause peaks in F to occur several seconds after the initial peak in pressure and C. After these two stages, three datasets were created each comprising sets of pressure data windows 216 s in duration centred on the times of the detections

and containing a signal expected to be from a Strombolian eruption at Erebus. Data gaps at one of the sensors can, when filtered, generate false detections due to high C values. However, these were easily identified; 95% of occurrences were removed by correlating with a typical artefact waveform.

3.4 CTBTO automated detection list

The CTBTO automatically generates event detection lists for all IMS stations and this could be an important data source for volcano researchers. To assess how they could be used, we determined how many of the 117 known Strombolian events were present on the automated CTBTO detection list for IS55. Each automatically detected event on the list has an associated arrival time, back-azimuth, trace velocity *(*apparent velocity of the wavefront across the array) and central frequency (frequency at which the signal has most energy compared to the noise), details which could be used to identify those CTBTO automatically detected events which are expected to be from Strombolian events at Erebus. The detection list was first reduced to only include those detections with back-azimuths between 330° and 340°, trace velocities of 320 to 350 m s^{-1} and detection times within 2 minutes of a known Strombolian event. Known Strombolian events included those from January 2006 and the additional known Strombolian events in February and March 2006 reported in Johnson et al. (2008). For those known Strombolian events that were also identified manually at IS55, the detection time listed in the CTBTO detection list was compared to the manually identified arrival time to check that they were within reasonable agreement. This first step enabled assessment of the capability of the CTBTO algorithm to detect Strombolian events at Erebus and also allowed calculation of the mean back-azimuth, apparent velocity and central frequency of those CTBTO automatic detections that were associated with known Strombolian events. Importantly, calculation of mean detection characteristics enabled identification of further detections in the CTBTO list that were expected to be due to Strombolian events at Erebus over the whole period of IS55 operation from 17 March 2004 to 31st December 2011.

4. Results

4.1 Infrasound from events manually identified at IS55

Of the 117 known Strombolian events (those detected locally by Jones et al., 2008) in January 2006, 75% were manually identified at IS55 by an analyst using methods described in section 3.2. The lowest amplitude recorded at SHK (ΔP_{shk}) of a known Strombolian event manually identified at IS55 is 6.6 Pa, leaving 17 known Strombolian events with ΔP_{shk} <6.6 Pa manually unidentifiable at IS55 (Table 2). All known Strombolian events with ΔP_{shk}> 232 Pa and 90% of known Strombolian events with ΔP_{shk} >25 Pa were identified manually at IS55. Only 26% of known Strombolian events with

ΔP_{shk} <25 Pa were identified manually at IS55, indicating that under typical conditions, propagation effects are too great for signals from such small Strombolian events at Erebus to consistently remain above the ambient infrasound noise levels at IS55. The frequency characteristics of infrasound from Strombolian explosions at Erebus are similar across a wide range of amplitudes (Rowe et al., 2000); therefore, using a single passband for detection should not affect signal identification at IS55. Those known Strombolian events with ΔP_{shk} >25 Pa that were not identified at IS55 are expected to have encountered unfavourable propagation conditions, or to have occurred during times of higher than typical ambient noise levels at IS55. The typical root mean squared ambient noise levels at IS55 over the period of study between 0.4 and 4 Hz is on the order 10^{-3} Pa. We note that IS55 can be considered a quiet station; at frequencies unaffected by the instrument response issues, IS55 is between a factor of two and five quieter than the median IMS noise characteristics (see curves of Matoza et al., 2013).

Table 3 Percentage of known Strombolian events manually identified at IS55 or associated with a CTBTO automatic detection as a function of amplitude at SHK. Note that the response of sensor SHK above 250 Pa is non-linear.

Amplitude range at SHK (Pa)	Number of events	Percentage of events identified manually at IS55	Percentage (and number) of events associated with CTBTO detections at IS55 (section 4.3)
0 – 5	17	0	12%
5 – 25	10	70%	50%
25 – 50	10	70%	50%
50 – 75	11	82%	82%
75 – 100	5	80%	100%
100 – 150	14	100%	93%
150 – 200	15	87%	100%
200 – 250	13	92%	85%
250 – 400	22	100%	100%

Measured peak-to-peak amplitudes of signals from known Strombolian identified at IS55 are positively correlated with the amplitudes measured at the local station RAY (Figure 4a). The amplitude of these events recorded at IS55 relative to those recorded at RAY varied between approximately 3% and 180% of the amplitude expected assuming the hemispherical spreading decay rate of $1/r$ where r is range from source (corresponding to between 0.04% and 2.4% of the amplitude recorded at RAY). The observed amplitude decay rate ranged from just over $1/r$ to approaching $1/r^2$; however, it increased and decreased relatively smoothly over time periods of a few days (Figure 4c). Propagation time between the local station SHK and IS55 decreased with

increasing amplitude decay rate (Figure 4b) indicating that conditions along the propagation path that affect propagation time must also have an influence on the amplitude decay rate.

In the calculations above, absorption of acoustic energy has been ignored because at the relatively short distances and low signal frequencies in this study, the absorption effects will be negligible. Over the 25km path, and for frequencies less than 8 Hz, absorption will reduce the amplitudes by less than 0.5% (Sutherland and Bass, 2004).

The correlation between waveforms recorded at an individual sensor is high, as can be seen qualitatively in Figure 5. The infrasonic signals of the 88 known Strombolian events that were identified at IS55 were cross correlated with each other at each local sensor and at IS55. Signals recorded at the local stations have mean correlation coefficient values between 0.88 and 0.89, whilst between signals recorded at IS55, the mean correlation coefficient value is only 0.7. The lower value for signals recorded at IS55 is likely to be due to a combination of lower SNR and time-varying propagation effects.

4.2 Automated detection of activity at Erebus for volcano monitoring

Though the amplitude of infrasound signals recorded at IS55 may be an unreliable indicator of the source amplitude of volcanic events at Erebus, a high proportion of the known Strombolian events at Erebus were identified manually at IS55 indicating that the array can be used to effectively monitor levels of activity at Erebus in terms of the frequency of occurrence of Strombolian events. Towards this aim, a methodology was developed to automatically detect events (Section 3.3). During the initial test period of January 2006 the F-detector, which identifies coherent signals irrespective of the shape of those waveforms, was found to out-perform the other methods. However, when the whole of 2006 was investigated it became clear that January 2006 was a relatively “quiet” time, when a relatively high proportion of the coherent infrasound signals detected at IS55 arriving from the direction of Erebus appeared to be associated with Strombolian eruptions. Over other periods during 2006 a higher proportion of coherent infrasound arriving at IS55 from the direction of Erebus did not have the waveform shape expected for Strombolian eruptions. Over the whole of 2006, the FC-detector was therefore found to be the most suitable detector because it is not only able to automatically detect coherent signals, but also those with a specific waveform shape. For this reason only the FC-detector will be discussed further in the main text but the performance of each of the detectors is discussed in greater detail in Appendix B.

The thresholds chosen to trigger automatic event detection depend on the application. High thresholds are suitable if automatic event detection is for research purposes when only high SNR events are wanted and a relatively low rate of successful detection (hit rate) is acceptable. However, if the purpose is to monitor volcanic activity for the safety of a local community, thresholds might be lower to prioritise a high hit rate over a low numbers of False Positives (FPs – noise or unwanted signals incorrectly identified as Strombolian events). Two pairs of thresholds (F_{TH} and C_{TH}) were chosen for FC-detector investigation, each with F_{TH}=16, but different C_{TH}: C_{TH}=0.7 to produce a low number of FPs, and C_{TH}=0.4 to give a higher hit rate but with a correspondingly higher number of FPs. These thresholds give differing automated detection rates. For C_{TH}=0.4 and F_{TH}=16, 63% of the known Strombolian events were automatically detected at IS55, compared to 75% manually identified by an analyst. For known Strombolian events that had ΔP_{IS55}>0.1Pa, 72% of the known Strombolian events that had been manually identified were detected automatically. For the higher correlation threshold (C_{TH}=0.7, F_{TH}=16) 54% of the known Strombolian events were automatically detected, with 71% of these events with ΔP_{IS55}>0.1Pa being detected automatically.

4.2.1. Automatic detection over 2006

Once detector performance had been assessed, the FC-detector was applied to data from the whole of 2006 to automatically detect signals expected to be from Strombolian events at Erebus. The FC-detector produced 530 automatic detections over the 2006 period using C_{TH}= 0.4, and 320 using C_{TH} = 0.7. Figure 6 shows how many signals are detected each week over the course of 2006. For comparison, data from Knox (2012) are also shown. Knox (2012) automatically detected signals expected to be Strombolian events at Erebus using cross correlation with a typical set of waveforms of both seismic and infrasonic data recorded locally. Due to the use of local data, we expect the signals detected by Knox (2012) to be a good representation of activity levels at Erebus. When weekly signal detection counts using the FC-detector are compared to those of Knox (2012), general trends in the frequency of signal detection compare favourably (Figure 6). Both datasets show a decrease in weekly signal detection counts in early 2006 from an average of approximately 30 per week to approximately 10 per week. Though not all events detected by Knox (2012) are expected to be detectable at IS55, as is shown to be the case in Figure 7, the automated weekly signal detection counts using F_{TH} = 16 and C_{TH} = 0.4 provide a good representation of activity levels at Erebus. Also evident from Figure 7 are a small number of occasions when more signals are automatically detected at IS55 than by Knox (2012) which may indicate periods where local stations were suffering down time (Figure 6) and data from IS55 provide a more complete record. Threshold values of F_{TH} = 16 and C_{TH} = 0.7 excluded all but the highest SNR lava lake explosions but the background trend in

activity levels is preserved. Though the higher FC-detector threshold values may not be suitable for monitoring activity at Erebus as so many of the events are not detected, they could provide a high quality dataset for research purposes, for example acoustic propagation studies.

4.3 Using CTBTO detections to monitor volcanic activity

Of the 117 known Strombolian events in January 2006, 74% were associated with a detection in the CTBTO automated detection list for IS55. Table 3 shows the details of the number of known Strombolian events that are associated with a CTBTO automatic detection as ΔP_{SHK} increases. Overall, 26% of known Strombolian events with $\Delta P_{SHK} \leq 25$ Pa were associated with a CTBTO automatic detection, whilst amongst known Strombolian events with $\Delta P_{SHK} > 25$ Pa the value increases to 88%. All of the known Strombolian events with $\Delta P_{SHK} \geq 244$ Pa were associated with a CTBTO automatic detection.

The characteristics of all CTBTO automatic detections that were associated with a known Strombolian event were catalogued. The mean and two standard deviation values for back-azimuth, central frequency and apparent velocity are 336.6±1.2°, 1.8±0.38 Hz and 0.329±0.007 km s^{-1}, respectively. Eighty percent of CTBTO detections associated with Strombolian events at Erebus have values for all three parameters within two standard deviations of their respective means. Using these two standard deviation values as maximum and minimum thresholds, the full CTBTO detection list for the period 17th March 2004 to 31st December 2011 was filtered to include only those automatic detections with characteristics expected to be associated with Strombolian events at Erebus.

The full CTBTO automatic detection list for IS55 for the period from the 17th March 2004 to the 31st December 2011 comprised over 330,000 detections. When these were filtered to include only those with the specified characteristics expected of detections associated with Strombolian events at Erebus, the number of detections decreased to 4,209 with between 0 and 137 per week and 0 and 295 per month. In January 2006, 105 CTBTO detections matched the filter criteria described above, but only 91 of these are associated with known Strombolian events. The remainder must be related either to Strombolian events that were not included in the original database of locally detected Strombolian events, other sources unrelated to the volcano or other volcanic activity at Erebus, though instances of the latter being detected at IS55 are rare. For example, Jones et al. (2008) found that of the volcanic infrasound signals detected proximally at Erebus during January to March 2006, more than 90% were Strombolian explosions. The remainder were classified as “ash venting”

events" and had relatively low amplitudes compared to Strombolian explosions leading them to be much less likely to be detected at IS55. Many of the weekly and monthly detection counts are greater than the expected number of Strombolian events at Erebus. For example, the period from late 2005 to early 2006 is recognised as a period of heightened activity, with monthly locally detected Strombolian event counts peaking at approximately 128 (Jones et al., 2008). In comparison, monthly detections using the filtered CTBTO automatic detection list are regularly greater than 100 for the whole period of station operation. There are broad similarities between the filtered CTBTO automatic detections and the dataset of Knox (2012, Figure 8). For example, in both datasets a heightened period of activity is evident between late 2005 and early 2007 with a decrease in activity during mid-late 2006. Unfortunately, there are also some very high peaks in the number of weekly filtered CTBTO automatic detections and many of these detections are unlikely to be related to activity at Erebus even though they exhibit the specified characteristics. Overall, although periods of heightened activity at Erebus are visible in the filtered CTBTO automatic detection list, large fluctuations in the numbers of apparent false detections make the dataset unreliable alone as an indicator of activity levels at Erebus.

5. Propagation effects observed in data from IS55

If infrasound monitoring and studying of volcanoes at near-regional distances is to become more commonplace in volcanology, the effects of atmospheric acoustic propagation on signals at these ranges and in several different environments need to be evaluated, as has been undertaken by e.g., Fee and Garces, (2007), Matoza et al., (2009), and Johnson et al., (2012). At Erebus we have the rare opportunity to compare data recorded near the vent to that recorded at a distance of 25km.

At near-regional ranges acoustic propagation between the source and receiver occurs within the troposphere. The acoustic amplitude recorded at an instrument located on Earth's surface is controlled by the magnitude of upward acoustic refraction along the path, balanced by any refraction of energy back towards Earth's surface within acoustic waveguide structures. The upward refraction is controlled by the reduction in effective sound speed (c_{eff}) with altitude, where c_{eff} is the sum of the adiabatic sound speed (a function of temperature) and the along-path wind speed (e.g., Evers and Haak, 2010). The more rapidly the temperature, and hence the effective sound speed, decreases with altitude the more upward refraction occurs, generating an acoustic shadow zone at far-regional distances (e.g., Piercy et. al., 1977). Since the dominant wind direction in the Ross Island area is from south to north (Monaghan et al., 2005; Seefeldt et al., 2003), counter to the direction of infrasound propagation from Erebus to IS55 causing a decrease in effective sound speed with

altitude, upward sound refraction is likely to be a common effect observed at IS55. It is not surprising therefore that amplitude decay rates observed at IS55 are predominantly greater than the $1/r$ rate predicted for hemispherical spreading.

At Erebus, as is often the case in volcanic scenarios, the near-regional recording station is located at a lower altitude than the explosion generating the infrasound; IS55 is located at 40m above sea level (a.s.l.), compared to station RAY at 3770m a.s.l. This can help combat the acoustic loss due to the upward refracting nature of the atmosphere, as a portion of the acoustic wavefield is diffracted around the vent region and travels downwards from the source, following the topography. Matoza et al. (2009) and Johnson et al. (2012) model such a phenomenon for infrasound arrivals observed many kilometres away from Mt St Helens and Volcan Villarrica, respectively.

Refraction of acoustic energy from significant increases in effective sound speed at the tropopause (i.e., within tropospheric acoustic waveguides) can occur in some geographical locations. This can result in the return of significant acoustic energy to surface instrumentation. There is no evidence of such atmospheric structure above Erebus in meteorological data collected by radiosondes released every 12 hours from the McMurdo station, located approximately 25km South-West of IS55 (Figure 2). This is in agreement with climatological models of the region (e.g., HWM07, Drob et al., 2008).

The most striking result is the relatively smooth temporal variation of amplitude decay rates and the relationship with propagation time (Figure 4c). These changes in amplitude decay rate are linked to changes in effective vertical sound speed gradient with time. This is shown using meteorological data collected by the McMurdo radiosondes released every 12 hours. From the radiosonde measurements of temperature and wind speed, the effective sound speed, c_{eff}, can be calculated.

The difference in c_{eff} between the altitudes of station RAY (3766m a.s.l.) and IS55 (41m a.s.l.), c_{eff}^{RAY}-c_{eff}^{IS55}, is used as a proxy for the vertical effective sound speed gradient. As expected, this gradient is always negative (Figure 9); the effective sound speed is less at the higher altitude of RAY due to the reduction in temperature and the higher amplitude winds counter to the propagation direction. Therefore upward refraction of sound is expected. Moreover, the changes in c_{eff}^{RAY}-c_{eff}^{IS55} are correlated with the changes in amplitude decay rate (Figure 9), showing that for the case of Erebus and IS55 the order of magnitude variation in amplitude can be attributed to changes in the effective sound speed gradient of approximately 3 m s^{-1} per kilometre of altitude. A greater understanding of this effect might be developed using numerical acoustic propagation modelling, as has been

undertaken by studies at other volcanoes (e.g. Matoza et al., 2009, Johnson et al., 2012 and Lacanna et al., 2014). For example, Johnson et al. (2012) found that the contrasting situation of increasing effective sound speed with height at Volcan Villarrica caused sound to efficiently refract back to the ground producing higher local-local amplitude ratios than seen at Erebus. However, a comparable study at Erebus would require substantial further work and is therefore outside the scope of this paper.

The general increase in propagation time with decreasing IS55/RAY amplitude ratio (Figure 4b) is also consistent with the meteorological data. At times of decreased effective sound speed gradient (when upward refraction is minimised and hence amplitude ratio is increased), increased average effective sound speed across the 0 to 3.8 km altitude range is observed. At these times, more rapid acoustic propagation leads to minimum propagation times.

At Erebus we have linked changes in propagation conditions to meteorological observations derived from the McMurdo radiosonde data. However, not all monitored volcanoes will have nearby meteorological data, such as these. In these cases it would be useful to try and identify the propagation conditions (i.e., the effective sound speed gradient) from some measure at the recording stations. Although wind speed and direction are recorded at IS55, no relationship was found between the along-path wind speed component and the signal amplitude decay rate. This suggests that surface wind speeds recorded at IS55, at 25km from and approximately 3 km below the vent, are not representative of conditions along the propagation path, limiting the usefulness of these data for predicting signal amplitude decay rates. However, at times of increased background noise at station SHK, high amplitude decay rates between the vent and IS55 are observed (Figure 10). It is has been well documented that there is a relationship between wind speed and RMS background infrasonic noise amplitude (e.g., Le Pichon et al., 2009). Consistent with this is the fact that many of the higher amplitude known Strombolian events not identified at IS55 occurred during times of higher than average background noise at SHK, indicating higher wind speeds. Although we cannot determine wind direction from infrasound noise measurements, it is likely that due to prevailing meteorological conditions these higher wind speeds will be counter to the propagation direction thereby increasing upward acoustic refraction. The implication of this result is that at Erebus it is the meteorological conditions close to the vent that dominate the observed amplitude decay rate. In areas of high relief, and complex topography, as are often found in volcanic regions, these conditions may be significantly different to those found at the recording station. Hence at some volcanoes it will be desirable to have constraints on the meteorological conditions close to the

vent in addition to the monitoring station to aid quantitative interpretation of near-regional infrasound recordings.

6. Wider implications of this study and conclusions

Although the 25 km distance between the IS55 infrasound array and the Strombolian eruptions at Erebus is much greater than ideal for monitoring low intensity volcanic activity, comparing IS55 infrasound data with abundant available local data has led to important insights into the effects of infrasound propagation at local-ranges. 75% of all events in a database of known Strombolian explosions at Erebus were identified manually by an analyst in infrasound data recorded at IS55. The lowest amplitude recorded at SHK (ΔP_{shk}) of a known Strombolian event which was identifiable at IS55 was 6.6 Pa. 26% of known Strombolian events with ΔP_{shk} below 25 Pa were identified at IS55 compared to 90% of known Strombolian events with ΔP_{shk} equal or greater than 25 Pa. More explosive eruptions that produce taller eruption plumes also produce infrasound with greater amplitudes that is detectable at greater distance (Dabrowa et al., 2011). Therefore, more explosive volcanoes will clearly be more suitable for monitoring at near-regional ranges. For example, the maximum amplitudes recorded at a distance of 3.2 km from Augustine during its eruption in 2006 were approximately 2000 Pa when reduced to a distance of 300 m using a conservative decay rate of $1/r$ (Petersen et al., 2006), an order of magnitude greater than typical high amplitude Strombolian events at Erebus.

Infrasound signals from known Strombolian events recorded at IS55 were, as expected, reduced in amplitude compared to recordings from local stations. Although the amplitudes recorded at IS55 correlate to some degree with those recorded locally, the relative amplitude recorded at IS55 compared to the local station RAY varies by up to a factor of 40 over the course of a few days. This is shown to be a propagation effect, controlled by the level of upward acoustic refraction generated by the meteorological conditions at the time of each explosion. Estimates of local amplitudes calculated from amplitudes at IS55 are therefore unreliable. Johnson et al. (2012) also found that amplitude decay rates varied greatly over a period of days at Villarrica, Chile, even at relatively close range: Amplitudes recorded at an array located approximately 8 km from the crater varied between 40 and 120% of that expected assuming hemispherical spreading from summit microphones, compared to variations of between 3 and 180% in our study.

Although the variability in amplitude decay rates observed at Erebus is extremely large (between 3 and 180% of that expected for hemispherical spreading), this variation is less than the four orders of

magnitude change in near-regionally recorded (range=37 km) acoustic amplitude observed at Tungurahua, Ecuador, as the activity changed from vigorous Strombolian activity to Plinian eruptions (Fee et al., 2010b). In this case, array deployments were specifically designed to target large-amplitude eruption signals. None the less, it implies that if a monitoring system is deployed to identify large changes in eruptive behaviour, the local propagation effects, although large, will not mask the source amplitude variability.

Both the radiosonde data and the use of background infrasonic noise levels at summit station SHK indicate that the amplitude decay rates experienced by infrasound propagating to IS55 depend on the along-path effective sound speed gradient. In addition, the observation that amplitude decay rates were not correlated with wind measurements at IS55 shows that meteorological measurements made only at the receiving station do not necessarily contain information about the propagation path. Indeed, if the station has been successfully sited to minimise noise levels, rather than maximise signal-to-noise ratios, it is likely that the contribution of the local wind field to the noise will have been minimised. This is the case for IMS stations that are designed in order to detect small amplitude signals from all directions of arrival. In summary, our Erebus results, like those of Matoza et al. (2009) for Mount St. Helens, indicate that to correct infrasound amplitude measurements at near-regional distances for the effect of propagation requires detailed knowledge of the effective sound speed profile along the path.

Although amplitudes recorded at IS55 are unreliable indicators of amplitudes near the vent, a large proportion of known Strombolian events detected locally were detectable at IS55. This means that the array could be used to monitor activity levels at Erebus in terms of the frequency of event occurrence. A method of automatically detecting infrasonic signals expected to be from Strombolian events at Erebus was developed exploiting both the coherence of infrasound from Erebus across the IS55 array and the similarity of infrasound signals from Strombolian explosions. Infrasound data recorded at IS55 over the period 1st January 2006 to 31st December 2006 were searched automatically for infrasound signals expected to be from Strombolian events. When compared to a database of weekly signal detection counts compiled using local seismic and infrasound data (Knox, 2012), the number of signals automatically detected at IS55 using our methodology was found to be a reliable indicator of activity levels at Erebus. A dataset based on infrasound data recorded at IS55 could therefore prove a useful resource during times of power outages or equipment failure at local instrumentation.

Though a number of studies have utilised IMS infrasound data for investigation of volcanic eruptions (e.g. Fee et al., 2010b, Matoza et al., 2011), the CTBTO detection lists have not yet been exploited and could be a useful resource for researchers. The CTBTO automated detection algorithm detected 78% of events in our database of known Strombolian explosions at Erebus. Using the characteristics of these detections as a filter, the entire record of CTBTO automatic detections at IS55 for the period 17th March 2004 to 31st December 2011 was filtered to search for detections which had characteristics similar to those expected to be associated Strombolian events. Although periods of increased activity at Erebus can be identified from these results, there are many time periods where a large proportion of the detections are unlikely to be due to activity at Erebus alone. Therefore the CTBTO automatic detection lists may not be reliable for monitoring volcanoes without additional processing. However, the high proportion of known Strombolian events that were detected indicates that CTBTO detection lists could be useful for researchers. For example, if a station is known to regularly detect infrasound from a particular volcano, CTBTO detection lists could be used to efficiently identify time windows worthy of further investigation, or in the case of a large eruption they could guide researchers to focus on data from particular IMS stations.

This study highlights that if infrasound data recorded at ranges of 10s of kilometres from the vent is to be used for detailed quantitative analysis, the effect of local meteorology should be taken into account before signal amplitudes can be interpreted in terms of source processes. Where local measurements are not available (such as the radiosonde data available for this study) then researchers could instead consider using atmospheric specifications derived from numerical weather prediction models. Our study found that at Erebus, amplitudes recorded at near-regional ranges provide an estimate of acoustic source strength that are accurate to within approximately an order of magnitude.

Appendix

A. Details of times and amplitudes of Strombolian events recorded at SHK

Table A1. Timings and peak-to-peak amplitudes (data filtered between 0.25 Hz and 20 Hz) of the 117 known Strombolian events in January 2006 at Mount Erebus recorded locally and used extensively for comparison in this study. The dataset is a modified subset of those presented in Figure 11 of Johnson et al. (2008). The dataset has been modified to correct for a mismatch between the reported event time and peak-to-peak amplitude in Johnson et al. (2008).

Event date and time					ΔP_{SHK}(Pa)
Year	Month	Day	Hrs.	Mins.	
2006	1	6	6	1	57.2
2006	1	6	16	7	108.1
2006	1	6	16	21	155.8
2006	1	6	22	39	227.6
2006	1	7	1	59	111.7
2006	1	7	2	36	0.7
2006	1	7	5	12	115.4
2006	1	7	9	13	28.0
2006	1	7	13	9	26.4
2006	1	7	17	56	241.8
2006	1	7	19	30	229.0
2006	1	7	21	4	0.9
2006	1	7	23	4	163.6
2006	1	8	8	19	279.7
2006	1	8	12	4	66.7
2006	1	8	15	25	227.1
2006	1	8	15	59	0.7
2006	1	8	19	55	307.2
2006	1	9	10	21	31.0
2006	1	9	11	15	21.5
2006	1	9	13	9	125.7
2006	1	9	14	8	159.0
2006	1	9	14	26	209.7

Event date and time					ΔP_{SHK}(Pa)
Year	Month	Day	Hrs.	Mins.	
2006	1	20	6	5	1.4
2006	1	20	6	47	1.4
2006	1	20	10	12	0.8
2006	1	20	16	5	263.6
2006	1	20	16	9	3.5
2006	1	21	3	12	2.7
2006	1	21	8	43	231.1
2006	1	21	12	34	89.0
2006	1	21	17	11	231.9
2006	1	21	17	13	22.4
2006	1	21	19	48	244.4
2006	1	22	2	53	33.3
2006	1	22	7	34	333.9
2006	1	22	7	36	54.9
2006	1	22	9	2	110.8
2006	1	22	9	3	52.4
2006	1	22	11	9	182.0
2006	1	22	21	2	2.4
2006	1	22	23	39	178.1
2006	1	23	9	49	161.7
2006	1	23	11	25	109.9
2006	1	23	15	19	40.7
2006	1	23	16	40	179.6

2006	1	9	17	34	132.5
2006	1	10	4	8	189.8
2006	1	10	9	15	329.0
2006	1	10	13	6	100.4
2006	1	10	19	19	310.5
2006	1	10	21	13	179.0
2006	1	11	8	54	21.1
2006	1	11	18	20	88.5
2006	1	11	20	52	47.7
2006	1	12	4	0	228.7
2006	1	12	8	9	296.1
2006	1	12	15	11	34.0
2006	1	12	20	9	55.0
2006	1	12	20	54	113.4
2006	1	13	5	4	91.7
2006	1	13	9	39	71.0
2006	1	13	10	21	325.6
2006	1	13	12	20	148.4
2006	1	13	16	36	34.3
2006	1	13	17	13	60.1
2006	1	13	19	23	340.3
2006	1	15	1	11	11.1
2006	1	15	8	42	386.9
2006	1	15	12	26	79.4
2006	1	15	20	59	172.6
2006	1	17	1	21	377.7
2006	1	17	16	56	1.3
2006	1	17	17	11	1.7
2006	1	17	17	30	1.6
2006	1	17	18	48	21.5
2006	1	18	15	11	273.4
2006	1	18	20	50	356.3
2006	1	18	20	51	231.6

2006	1	23	19	59	121.4
2006	1	24	2	0	8.5
2006	1	24	2	9	198.1
2006	1	24	4	32	314.7
2006	1	24	9	10	128.6
2006	1	24	16	20	61.3
2006	1	24	23	17	159.1
2006	1	24	23	24	227.6
2006	1	25	6	58	262.2
2006	1	25	18	10	313.9
2006	1	26	8	14	276.2
2006	1	26	14	16	88.5
2006	1	27	11	26	2.0
2006	1	27	12	29	152.6
2006	1	27	17	49	43.6
2006	1	27	19	30	212.2
2006	1	28	3	5	25.6
2006	1	28	5	47	164.1
2006	1	28	7	49	235.6
2006	1	28	12	41	84.2
2006	1	28	23	27	337.8
2006	1	29	17	11	2.5
2006	1	29	18	2	299.8
2006	1	30	4	53	68.1
2006	1	30	9	59	61.1
2006	1	30	10	33	10.8
2006	1	30	17	9	343.3
2006	1	30	19	11	110.1
2006	1	31	4	14	14.9
2006	1	31	6	16	20.3
2006	1	31	11	20	6.6
2006	1	31	12	3	370.8
2006	1	31	19	56	3.4

2006	1	19	18	54	188.2
2006	1	19	19	42	128.2
2006	1	20	1	55	271.4

2006	1	31	22	7	1.0
2006	1	31	23	40	2.2

B. Assessing automatic detectors

Methods of automatically detecting signals expected to be from Strombolian events at Erebus were developed using threshold values of either the F-statistic value of the beamed data (the F-detector), the value of the correlation coefficient between the beamed data and a typical lava lake explosion waveform (the C-detector), or both (the FC-detector). To evaluate each detector and each threshold value, the number of true detections (instances where a signal from a known Strombolian event is correctly detected, commonly termed hits) and the number of false detections (instances where noise is incorrectly identified as a signal from a Strombolian event) had to be determined. For evaluation, the detectors were run using data from January 2006, a period during which the manually identified arrival times at IS55 of signals from known Strombolian events (defined as the time of the first peak in pressure) were known accurately and could be compared to the automated signal detection times. As such, the detectors were assessed against a human analyst.

Detections from the C-detector and FC-detector (D_C and D_{FC} respectively) were classified as a hit if they fell within ±0.5 s of a manually identified arrival time for a known Strombolian event. As described in section 3.3, peaks in F generally occurred slightly after the true arrival time and the F variable has a lower time resolution. Therefore detections from the F-detector were identified as a hit if their time was within -2 to +10 seconds of a manually identified event time. All other detections were classified as false positives. If more than one detection fell within the allowed time window, the detection closest in time to the corresponding event time was retained as a hit, and all others re-classified as false positives.

Each method was assessed using Receiver Operator Characteristic (ROC) curves (e.g. Arrowsmith et al., 2009). These exploit the fact that for a binary detector (where each data point in the whole series is defined as either a detection or noise) there are four possible outcomes. A true positive is the correct detection of a real event (a hit), a false positive (FP) is the detection of an event when there is none; a true negative is the correct detection of noise, and a false negative the miss-identification of an event as noise (a miss). A detector's effectiveness is defined by two parameters: its hit rate (number of hits divided by the total number of events) and its FP rate (number of FPs divided by the total potential number of FPs). ROC curves plot the hit rate against the FP rate for a detector at given threshold values and allow easy comparison of the performance of different detectors. For this study the total potential number of FPs was not defined and comparison of the number of FPs, rather than the rate of FPs, was sufficient because all three detector methods were assessed using identical data sets.

At the highest threshold levels tested, the number of FPs detected were low (<10% of the number of manually identified known Strombolian events), but hit rates were also relatively low, between approximately 62% and 74% of the manually identified known Strombolian events compared to between 84% and 98% at the lowest thresholds (Figure B1). However, at the lowest thresholds the number of FPs also increased, reaching values of hundreds of times the number of known Strombolian events using the F- and C-detectors. At the highest threshold levels investigated, four FPs were produced by C- and FC-detector and seven by the F-detector. Further investigation suggests that these apparent FPs may be due to Strombolian explosions that are missing from the list of known Strombolian events as the waveforms are all highly coherent, have high amplitudes and look qualitatively like Strombolian explosions. During analysis it was noted that at least some of the apparent FPs are signals that were closely spaced in time and perhaps were not classified as separate events by Jones et al. (2008). If true, this would mean the performance of the automated detectors are better than shown in Figure B1. However, manual inspection revealed that many of the signals classified as FPs at lower thresholds show no clearly identifiable signal and are interpreted as true FPs. Jones et al. (2008) compared their detected event list (used in this study) to that of the MEVO and found that although their methodology detected more events overall than the MEVO, some were detected exclusively by the MEVO and vice versa. It therefore seems possible that some of the apparent FPs at IS55 detected at the highest chosen thresholds are actually hits related to Strombolian explosions at Erebus not listed by Jones et al. (2008). Overall, the F-detector methodology (using F values only) out-performed the other two methods at all comparable threshold values for the time period of assessment (Figure B1) because for a given number of FPs the F-detector consistently produced the highest hit rate. Of the three detectors, the C-detector performed the most poorly and will not be discussed further.

Two thresholds or pairs of thresholds (F_{TH} and C_{TH}) were chosen for the F- and FC-detectors for further evaluation. To produce a low number of FPs a high value of F_{TH} = 24 was chosen for the F-detector, and F_{TH}=16, C_{TH}=0.7 for the FC-detector. To give a higher hit rate but with a correspondingly higher number of FPs, a value of F_{TH}=14 was chosen for the F-detector and F_{TH}=16, C_{TH}=0.4 for the FC-detector (Figure B1). Using the chosen thresholds, between 72% and 99% of the known Strombolian events identified manually at IS55, that had a $\Delta P_{IS55} \geq 0.1$ Pa were detected automatically (Table B3). Only 75% of the known Strombolian events used in this study had been identified manually at IS55. Taking this into account, the percentage of all the known Strombolian events that we detected automatically ranged from 54% to 74% (91% and 100% of 75% respectively;

Table B3). Full details of the percentage of events detected automatically both as a function of amplitude at IS55, and at SHK are given in Table B4 and Table B5.

Table B3. Detection results for the thresholds and methodologies chosen.

Detector	Threshold value(s)	Hit rate (%)	Number of FPs	FPs as % of total detections	% of January events detected overall
F	F_{TH}=14	96	21	12	72
	F_{TH}=24	79	7	8	59
FC	F_{TH}=16, C_{TH}=0.4	84	21	15	63
	F_{TH}=16, C_{TH}=0.7	72	6	5	54

Table B4 Details of the percentage of known Strombolian events identified manually that are also detected automatically, as a function of ΔP_{IS55}.

ΔP_{IS55} (Pa)	% detected using F_{TH}=14	% detected using F_{TH}=24	% detected using F_{TH}=16 and C_{TH}=0.4	% detected using F_{TH}=16 and C_{TH}=0.7
0 – 0.05	No events	No events	No events	No events
0.05 – 0.075	50	0	0	0
0.075 – 0.1	67	33	33	0
0.1 – 0.2	100	67	47	33
0.2 – 0.5	100	89	59	63
0.5 – 0.75	93	86	86	79
0.75 – 1.0	100	100	100	100
1.0 – 6.0	100	88	83	96

Table B5. Percentage of all known Strombolian events used in this study that were detected automatically as a function ΔP_{SHK}.

ΔP_{SHK} (Pa)	% detected using F_{TH}=14	% detected using F_{TH}=24	% detected using F_{TH}=16 and C=0.4	% detected using F_{TH}=16 and C=0.7
0 – 5	0	0	0	0
5 – 25	62	46	46	38
25 – 50	78	67	78	67
50 – 75	78	78	78	78
75 – 100	75	63	75	75
100 – 150	88	81	81	63
150 – 200	90	73	73	64
200 – 250	85	57	71	64
250 – 400	100	90	85	85

Both the F- and FC-detector were applied to data from the whole of 2006 to automatically detect events. Figure B2 shows the number of signals detected per week by both the F- and FC-detector over the whole of 2006. Using the F-detector the weekly signal detection counts were unfeasibly high to be related solely to Strombolian activity at Erebus. Values ranged from 0 and 180 and 0 to over 2000 with F_{TH}=22 and F_{TH} = 16 respectively. The F- detector was initially chosen because it out-performed both the C- and FC-detector over the assessment period (January 2006). However, it is clear that this period was a relatively quiet time at IS55 for the back-azimuths associated with Erebus and that during the majority of 2006 the performance of the F-detector is poor because it cannot distinguish Strombolian activity at Erebus from other unrelated coherent infrasound. In comparison the FC-detector is able to discern when infrasound recorded at IS55 has a similar waveform shape to that expected from Strombolian explosions and therefore was found to perform much better over the whole of 2006 (Figure 6). Consequently only the results of the FC-detector are discussed in the main text. It should be noted that the F-detector could be detecting other types of volcanic activity at Erebus as well as signals unrelated to the volcano. However, Strombolian explosions are by far the most frequent form of activity at Erebus (Jones et al., 2008) whilst other forms of activity additionally have low amplitudes compared to Strombolian activity and likely to be detected at IS55 only very rarely.

Acknowledgements

We thank David Fee and Robin Matoza for thorough, constructive reviews of the submitted manuscript. Their suggestions helped improve the paper. We thank Pierrick Mialle at the Comprehensive Nuclear-Test-Ban Treaty Organisation for providing IS55 data. We also thank David Fee and Tom Gabrielson for providing us with the measured infrasound system response for station IS55. The authors appreciate the support of the University of Wisconsin-Madison Antarctic Meteorological Research Center for the radiosonde data set and information (NSF grant ANT-1141908) and thank Hunter Knox for the additional detection dataset to which our data was compared (Knox, 2012). This work formed part of a PhD studentship funded as a NERC CASE partnership supported by NERC and AWE Plc; it was also supported by NERC grant NE/G016593/1.

References

Arrowsmith, S.J., Whitaker, R., Katz, C., Hayward, C., 2009. The F-Detector Revisited: An Improved Strategy for Signal Detection at Seismic and Infrasound Arrays. Bull. of the Seismol. Soc. of Am. 99, 1, 449-453.

Blandford.R, 1974. Automatic events detctor at Tonto-forest seismic observatory. Geophys. 39, 633-643.

Bowman, J.R., Baker, G.E., Bahavar, M., 2005. Ambient infrasound noise. Geophys. Res. Lett. 32, 9, L09803.

Brachet, N., Brown, D., Le Bras, R., Cansi, Y., Mialle, P., Coyne, J., 2010. Monitoring the earth's atmosphere with the global IMS infrasound network, in: Le Pichon, A., Blanc, E., Hauchecorne, A. (Eds.), Infrasound Monitoring for Atmospheric Studies. Springer, pp. 77 - 118.

Buckingham, M.J., Garces, M.A., 1996. Canonical model of volcano acoustics. J. of Geophys. Res.-Solid Earth 101, 8129-8151.

Campus, P., Christie, D., R., 2010. Worldwide Observations of Infrasonic Waves., in: Le Pichon, A., Blanc, E., Hauchecorne, A. (Eds.), Infrasound Monitoring for Atmospheric Studies. Springer, pp. 185 - 234.

Ceranna, L., Le Pichon, A., Green, D.N., Mialle, P., 2009. The Buncefield explosion: a benchmark for infrasound analysis across Central Europe. Geophys. J. Int. 177, 491-508.

Christie, D.R., Campus, P., 2010. The IMS infrasound network: design and establishment of infrasound stations, in: Le Pichon, A., Blanc, E., Hauchecorne, A. (Eds.), Infrasound Monitoring for Atmospheric Studies. Springer, Netherlands, pp. 29 - 75.

Dabrowa, A. L., Green, D. N., Rust, A. C., Phillips, J. C., 2011. A global study of volcanic infrasound characteristics and and the potential for long-range monitoring. Earth and Planet. Sci. Lett. 310, 369-379.

Dibble, R. R., 1989. Infrasonic recordings of Strombolian eruptions of Erebus, Antarctica, March – December 1984, covering the jump in activity on 13 September 1984, in: J. Latter (Ed.), Volcanic Hazards, assessment and monitoring. Springer-Verlag, Berlin, pp. 536-553.

Drob, D. P., Picone, J. M. and Garces, M., 2003. Global morphology of infrasound propagation. J. Geophys. Res., Vol. 108, No. D21.

Drob, D. P., et al, 2008. An empirical model of the Earth's horizontal wind fields: HWM07. Journal of Geophysical Research: Space Physics 113(A12304).

Evers, L. G. and Haak, H. W., 2010. The characteristics of infrasound, its propagation and some early history, in: Le Pichon, A., Blanc, E., Hauchecorne, A. (Eds.), Infrasound Monitoring for Atmospheric Studies. Springer, Netherlands, pp. 3 – 27.

Fee, D., Garces, M., 2007. Infrasonic tremor in the diffraction zone. Geophys. Res. Lett. 34, L16826.

Fee, D., Garces, M., Steffke, A., 2010b. Infrasound from Tungurahua Volcano 2006-2008: Strombolian to Plinian eruptive activity. J. of Volcanol. and Geotherm. Res. 193, 67-81.

Fee, D., & Matoza, R. S. (2013). An overview of volcano infrasound: From hawaiian to plinian, local to global. Journal of Volcanology and Geothermal Research, *249*, 123-139.

Freund, R.J., Wilson, W.J., 1997. Statistical Methods. Academic Press.

Gabrielson, T. B., 2011. *In situ* calibration of atmospheric-infrasound sensors including the effects of wind-noise-reduction pipe systems. J. Acoust. Soc. Am. 130(3), 1154-1163

Gerst, A., Hort, M., Kyle, P.R., Voge, M., 2008. 4D velocity of Strombolian eruptions and man-made explosions derived from multiple Doppler radar instruments. J. of Volcanol. and Geothermal Res. 177, 648-660.

Goto, A., Johnson, J.B., 2011. Monotonic infrasound and Helmholtz resonance at Volcan Villarrica (Chile). Geophys. Res. Lett. 38, 5.

Johnson, J. B., Anderson, J., Marcillo, O., Arrowsmith, S., 2012. Probing local wind and temperature structure using infrasound from Volcan Villarrica (Chile). J. Geophys. Res. 117, D017694.

Johnson, J., Aster, R., Jones, K.R., Kyle, P., McIntosh, B., 2008. Acoustic source characterization of impulsive Strombolian eruptions from the Mount Erebus lava lake. J. of Volcanol. and Geotherm. Res. 177, 673-686.

Jones, K.R., Johnson, J.B., Aster, R., Kyle, P.R., McIntosh, W.C., 2008. Infrasonic tracking of large bubble bursts and ash venting at Erebus Volcano, Antarctica. J. of Volcanol. and Geotherm. Res. 177, 661-672.

Knox, H., 2012. Eruptive characteristics and glacial earthquake investigation on Erebus volcano, Antarctica. Ph.D. Thesis, New Mexico Institute of Mining and Technology, p. 180.

Lacanna, G., Ichihara, M., Iwakuni, M., Takeo, M., Iguchi, M., Ripepe, M., 2014. Influence of atmospheric structure and topography on infrasonic wave propagation. J. of Geophys. Res.-Solid Earth. 119, 2988-3005.

Le Pichon, A., Vergoz, J., Blanc, E., Guilbert, J., Ceranna, L., Evers, L., Brachet, N., 2009. Assessing the performance of the International Monitoring System's infrasound network: Geographical coverage and temporal variabilities. J. of Geophys. Res.-Atmos. 114, 15.

Marchetti, E., Ripepe, M., Harris, A.J.L., Delle Donne, D., 2009. Tracing the differences between Vulcanian and Strombolian explosions using infrasonic and thermal radiation energy. Earth and Planet. Sci. Lett. 279, 273-281.

Matoza, R. S., Garces, M. A., Chouet, B. A., D'Auria, L. Hedlin, M. A. H., De Groot-Hedlin, C., Waite, G. P., 2009. The source of infrasound associated with long-period events at Mount St. Helens. J. of Geophys. Res., 114, B04305

Matoza, R. S., Fee, D., & Garcés, M. A. (2010). Infrasonic tremor wavefield of the Pu'u 'Ō'ō crater complex and lava tube system, Hawaii, in April 2007. Journal of Geophysical Research: Solid Earth (1978–2012), 115(B12).

Matoza, R.S., Le Pichon, A., Vergoz, J., Herry, P., Lalande, J.M., Lee, H.I., Che, I.Y., Rybin, A., 2011. Infrasonic observations of the June 2009 Sarychev Peak eruption, Kuril Islands: Implications for infrasonic monitoring of remote explosive volcanism. J. of Volcanol. and Geotherm. Res. 200, 35-48.

Matoza, R. S., Landès, M., Le Pichon, A., Ceranna, L., & Brown, D. (2013). Coherent ambient infrasound recorded by the International Monitoring System. Geophysical Research Letters, 40(2), 429-433.

Monaghan, A.J., Bromwich, D.H., Powers, J.G., Manning, K.W., 2005. The climate of the McMurdo, Antarctica, region as represented by one year of forecasts from the Antarctic Mesoscale Prediction System. J. of Clim. 18, 1174–1189.

Montalto, P., Cannata, A., Privitera, E., Gresta, S., Nunnari, G., Patane, D., 2010. Towards an Automatic Monitoring System of Infrasonic Events at Mt. Etna: Strategies for Source Location and Modeling. Pure and Appl. Geophys. 167, 1215-1231.

Neal, C., Girina, O., Senyukov, S., Rybin, A., Osiensky, J., Izbekov, P., Fergusson, G., 2009. Russian eruption warning systems for aviation. Nat. Hazards 51, 245-262.

Negraru, P.T., Herrin, E.T., 2009. On Infrasound Waveguides and Dispersion. Seismol. Res. Lett. 80, 565-571.

Oppenheimer, C., Kyle, P., 2008. Volcanology of Erebus volcano, Antarctica Preface. J. of Volcanol. and Geotherm. Res. 177, V-VII.

Oppenheimer, C., Lomakina, A.S., Kyle, P.R., Kingsbury, N.G., Boichu, M., 2009. Pulsatory magma supply to a phonolite lava lake. Earth and Planet. Sci. Lett. 284, 392-398.

Petersen, T., De Angelis, S., Tytgat, G., McNutt, S.R., 2006. Local infrasound observations of large ash explosions at Augustine Volcano, Alaska, during January 11-28, 2006. Geophys. Res. Lett. 33, L12303.

Piercy, J. E., Embleton, T. F. W. and Sutherland, L. C., 1977. Review of noise propagation in the atmosphere, J. Acoust. Soc. Am. 61(6), 1403-1418.

Ripepe, M., Marchetti, E., 2002. Array tracking of infrasonic sources at Stromboli volcano. Geophys. Res. Lett. 29, 2076.

Ripepe, M., Marchetti, E., Bonadonna, C., Harris, A.J.L., Pioli, L., Ulivieri, G., 2010. Monochromatic infrasonic tremor driven by persistent degassing and convection at Villarrica Volcano, Chile. Geophys. Res. Lett. 37, 6.

Rost, S., Thomas, C., 2002. Array seismology: Methods and applications. Rev. of Geophys. 40, 1008.

Rowe, C.A., Aster, R.C., Kyle, P.R., Dibble, R.R., Schlue, J.W., 2000. Seismic and acoustic observations at Mount Erebus Volcano, Ross Island, Antarctica, 1994-1998. J. of Volcanol. and Geotherm. Res. 101, 105-128.

Szuberla, C. A. L. and Arnoult, K. M. Locating explosions, volcanoes, and more with infrasound, Phys. Today 64(4), 74 (2011); doi:10.1063/1.3580503

Seefeldt, M.W., Tripoli, G.J., Stearns, C.R., 2003. A high-resolution numerical simulation of the wind flow in the Ross Island region, Antarctica. Mon. Weather Rev. 131,2, 435.

Sweeney, D., Kyle, P.R., Oppenheimer, C., 2008. Sulfur dioxide emissions and degassing behavior of Erebus volcano, Antarctica. J. of Volcanol. and Geotherm. Res. 177, 725-733.

Vergniolle, S., Boichu, M., Caplan-Auerbach, J., 2004. Acoustic measurements of the 1999 basaltic eruption of Shishaldin volcano, Alaska - 1. Origin of Strombolian activity. J. of Volcanol. and Geotherm. Res. 137, 109-134.

Vergniolle, S., Brandeis, G., 1996. Strombolian explosions .1. A large bubble breaking at the surface of a lava column as a source of sound. J. of Geophys. Res.-Solid Earth 101, 20433-20447.

Vergniolle, S., Caplan-Auerbach, J., 2004. Acoustic measurements of the 1999 basaltic eruption of Shishaldin volcano, Alaska - 2. Precursor to the Subplinian phase. J. of Volcanol. and Geotherm. Res. 137, 135-151.

Wilson, C.R., Szuberla, C.A.L., Olson, J.V., 2010. High-latitude observations of infrasound from Alaska: mountain associated waves and geomagnetic/auroral infrasonic signals, in: Le Pichon, A., Blanc, E., Hauchecorne, A. (Eds.), Infrasound monitoring for atmospheric studies. Springer, Netherlands, pp. 415 - 454.

Figure captions:

Figure 1 Signals detected at IS55 by the CTBTO over the period 1st January to 31st December 2006. Colour of data point indicates the central frequency of the signal detected (Hz); this is the frequency where the signal has the most energy when compared to the background noise. The prominent set of arrivals at a back azimuth of ~335 degrees is associated with detections from Erebus. Signals were detected using the PMCC (Progressive Multi-Channel Correlation) method (see section 3.1).

Figure 2 Location details for instruments used in this study. The location is shown of Mount Erebus and Ray Lake (triangle marker, a, b, and c), McMurdo station (star marker, b), the IMS infrasound array IS55 and its constituent pressure sensors (filled squares, b and d) and meteorological sensors

(open square, d), and the local stations SHK, RAY and E1S (filled diamonds, c) situated around Ray Lake.

Figure 3 Values of pressure, F and C as a signal arrives at IS55. Dotted vertical lines indicate the time of events at SHK (a-c), vertical dashed lines show the user defined approximate start and end time of the signal at IS55 (d) and horizontal dashed lines (e, f) indicate example threshold values of F and C which can be used to automatically detect events (section 3.3). Infrasound data in this figure are filtered between 0.1 and 4.45 Hz.

Figure 4 a) Amplitude recorded at IS55 25 km from the summit as a function of amplitude recorded at RAY 328 m from the centre of the lava lake b) IS55/RAY amplitude ratio as a function of propagation time and c) IS55/RAY amplitude ratio as a function of arrival time. In c) blue dashed lines indicate values expected for a 1/r (upper line) and $1/r^2$ (lower line) decay rates while right hand y-axis indicates values as % of that expected for a 1/r decay rate. Errors caused by instrument self-noise and ambient acoustic noise at the field sites are smaller than data markers in all cases.

Figure 5 All events identified manually at IS55 in January 2006 recorded at SHK, RAY, E1S and IS55 (a – d). All local data were filtered between 0.25 and 20 Hz whilst IS55 data is filtered above 0.25 Hz. It should be noted that the lower Nyquist frequency of IS55 data (sampling rate of 20 Hz) means signals recorded at this array will have reduced high frequency energy content compared to the local data. Stacked signals are shown as a thick black line. e) to h) show frequency characteristics of infrasound from event number 1 on 6th Jan at 16:07:46. Black lines indicate characteristics of the signal and grey lines the background noise. IS55 data were beamformed as described in section 3.2. Dashed blue and black lines indicate upper and lower values associated with a confidence level of 95%.

Figure 6 Comparison between weekly number of events detected a) automatically using infrasound data recorded at IS55 using FC-detectors and b) by Knox (2012) using local seismic and infrasonic data. In b) the black bars indicate the number events detected and the grey indicates the percentage of time the local station was operational. IS55 was operational 99.9% of the time.

Figure 7 Correlation between events detected in a given week by Knox (2012) and using our automated FC detection methods. Crosses indicate events detected using the lower C_{TH} whilst circles represent those detected using the higher C_{TH}

Figure 8 Comparison between the weekly number of CTBTO detections meeting the filter criteria (a) and b) show this data with different y-scales) and those events detected by Knox (2012) (c), modified from Knox, 2012). Note - IS55 was operational only from 17th March 2004 after which it was up >98% of time. Black bars indicate events per week; grey indicates local station up-time.

Figure 9 The left hand panel provides examples of the effective sound speed profile derived from the McMurdo radiosonde data for the Erebus to IS55 propagation direction. The four profiles are for midnight on 2006-Jan-08 (grey dashed), 2006-Jan-15 (grey), 2006-Jan-22 (black) and 2006-Jan-29 (black dashed). The altitudes of the two stations RAY and IS55 are indicated by the horizontal dotted lines. The right hand panel compares the signal amplitude ratios calculated from Erebus signals at RAY and IS55 (black line and dots) with the difference in effective sound speed at altitudes of RAY and IS55 (dashed line) during January 2006.

Figure 10 Influence of RMS background noise at SHK used as a proxy for wind speed. a) Event amplitude at SHK plotted against the corresponding RMS background noise amplitude at SHK. Events that were not identified manually at IS55 are highlighted with square markers. The mean value of pre-signal RMS noise amplitude is 0.45 Pa, indicated by a vertical line. b) Ratio of the amplitude at IS55 compared to RAY, compared to the RMS noise amplitude at SHK. Background noise amplitudes are calculated from unfiltered data. Error bars representing errors caused by ambient acoustic noise at the field sites are shown in a) as grey bars where visible whilst in b) these errors are smaller in all cases than the data markers. A dashed line represents the best fitting linear relationship between the markers.

Figure B1. ROC curves for 3 detectors automatically detecting Strombolian events at Erebus. Each data point represents the results using a particular threshold or pair of thresholds, with threshold values decreasing bottom-left to top-right. Results are shown for the F-detector, FC-detector and C detector (upper, middle and lower lines respectively). Threshold values of C (C_{TH}) ranged from 0.2 to 0.75 in increments of 0.05, whilst thresholds of F (F_{TH}) ranged from 2 to 30 in increments of 2. Filled squares highlight the thresholds chosen for further work. These are F_{TH}=14 or 24 using the F-detector and F_{TH}=16, C_{TH}=0.4 and F_{TH}=16, C_{TH}=0.7 using the FC-detector. For the FC-detector, only results for F_{TH}=16, C_{TH} = 0.2 to 0.75 are shown as F_{TH}=16 showed the best performance.

Figure B2 Weekly event counts using the F-detector (a) and FC-detector (b) to automatically detect events during 2006.

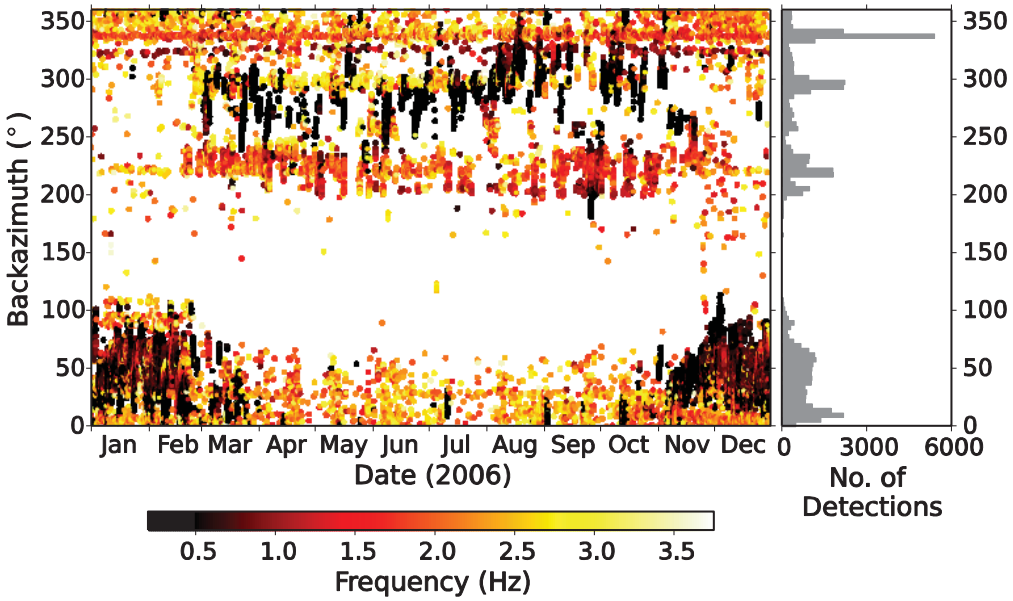

Figure 1

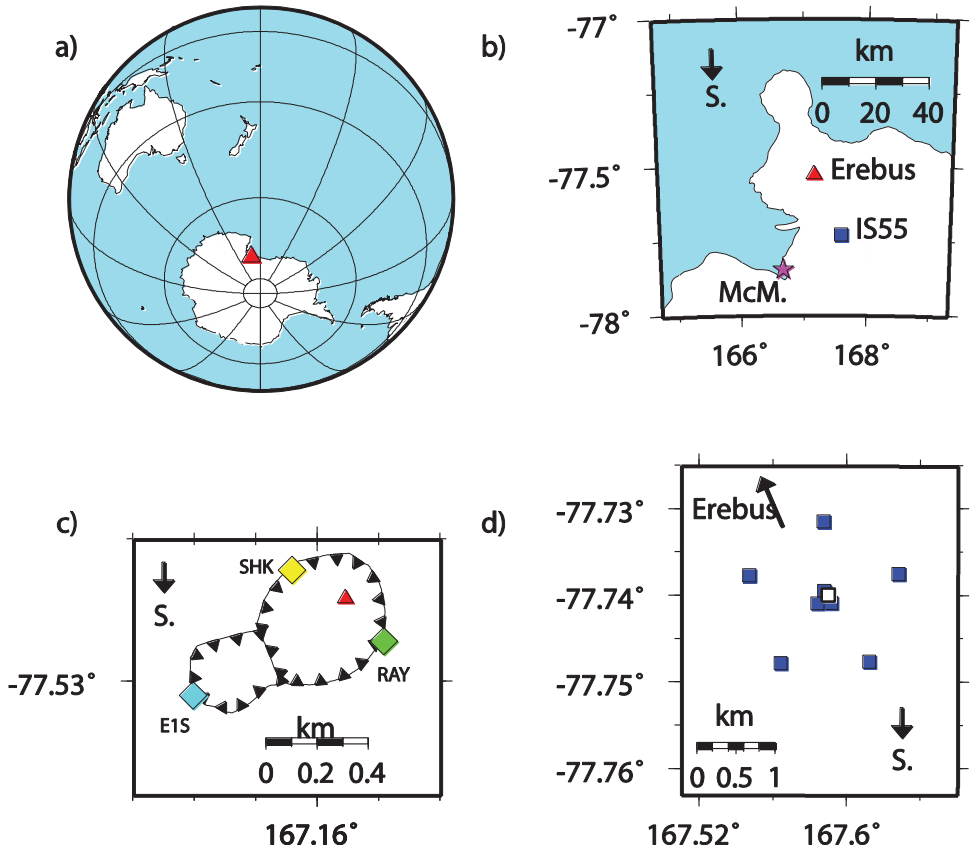

Figure 2

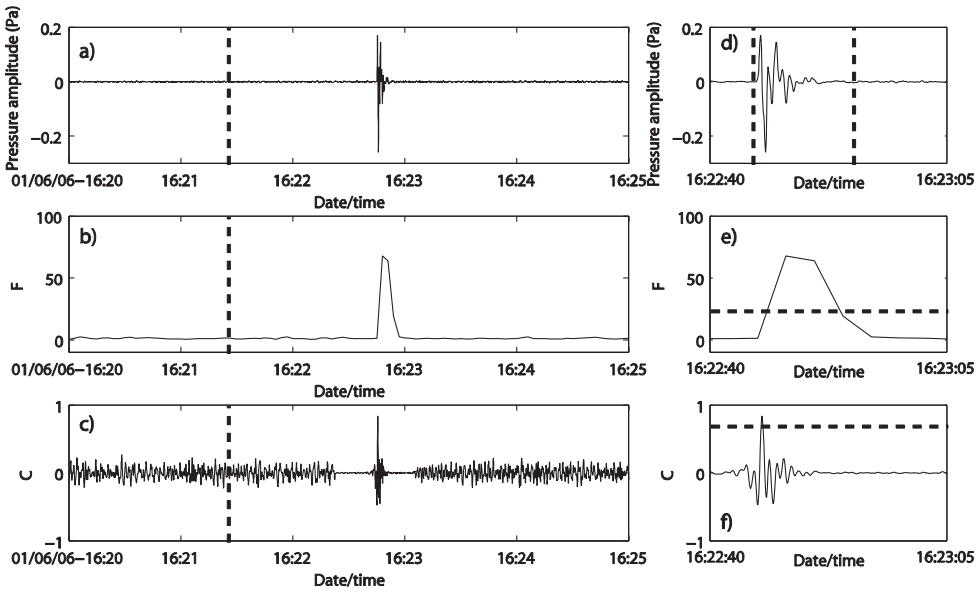

Figure 3

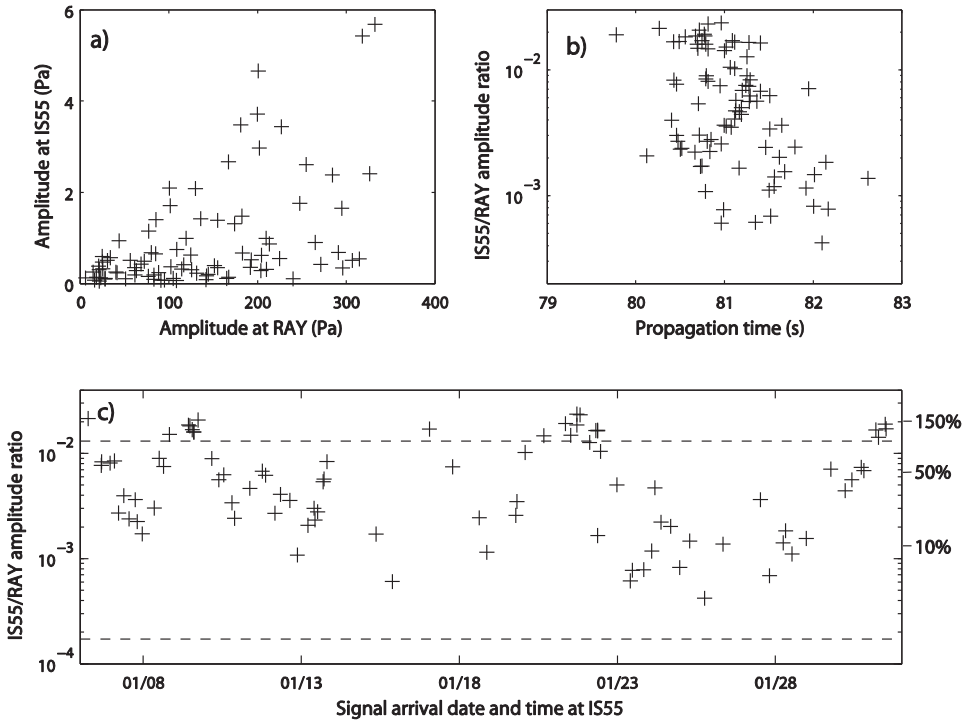

Figure 4

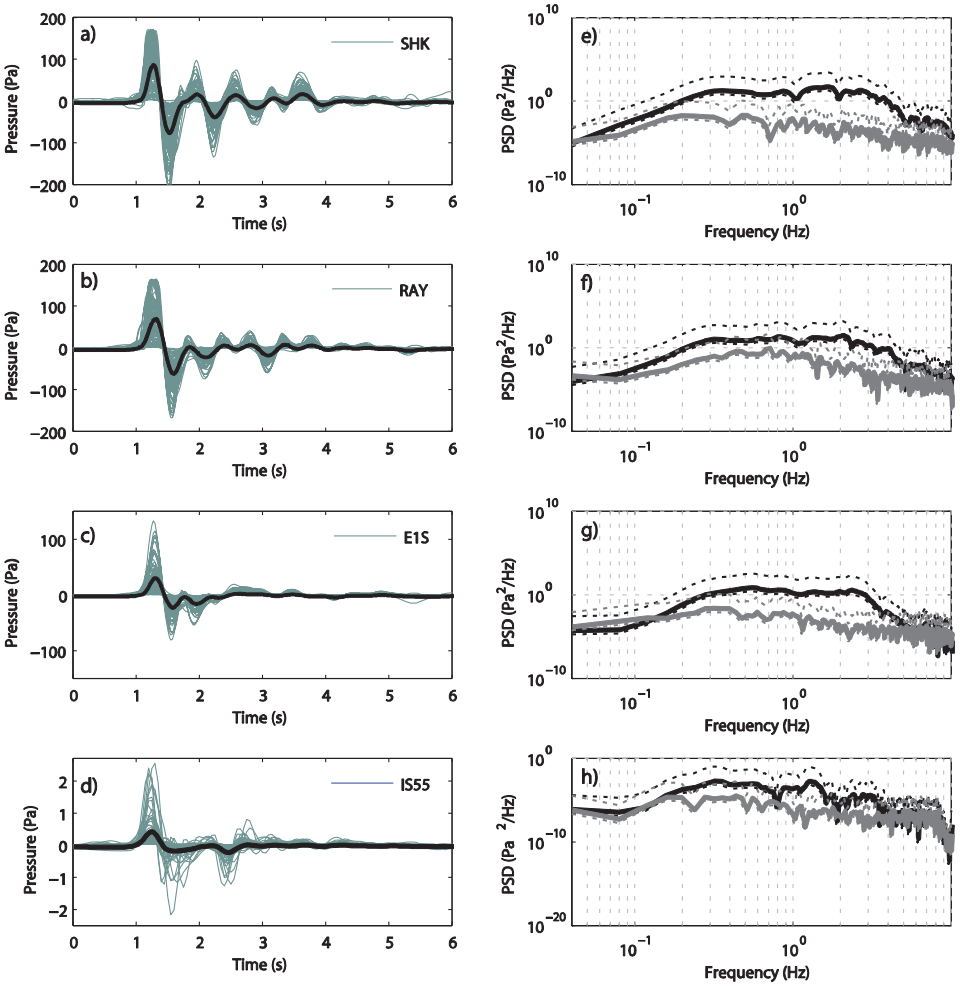

Figure 5

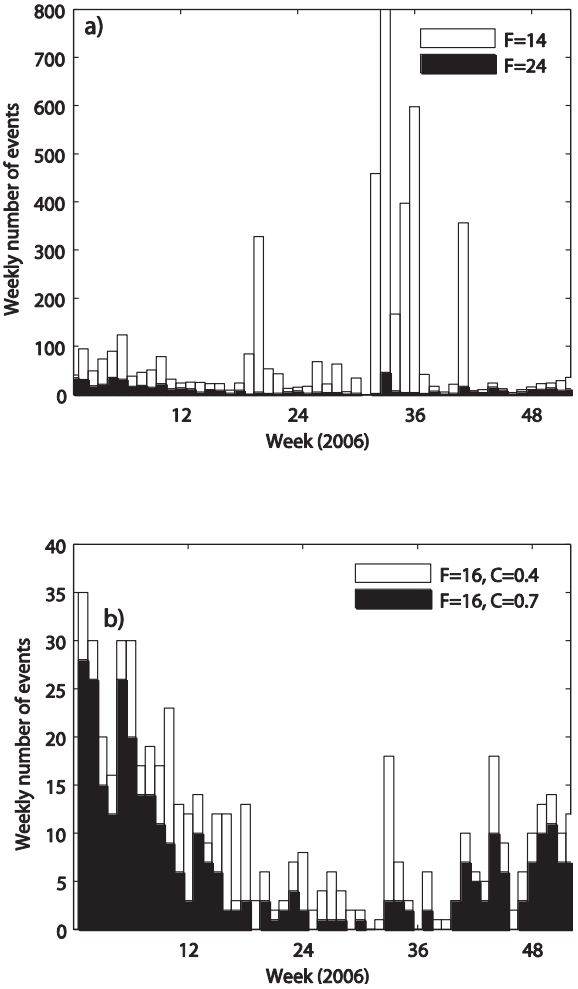

Figure 6

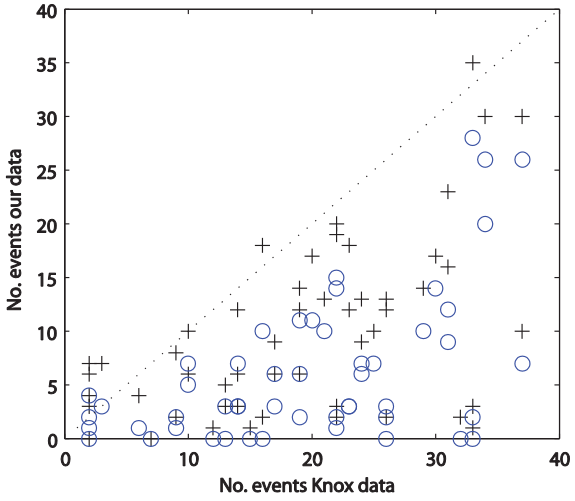

Figure 7

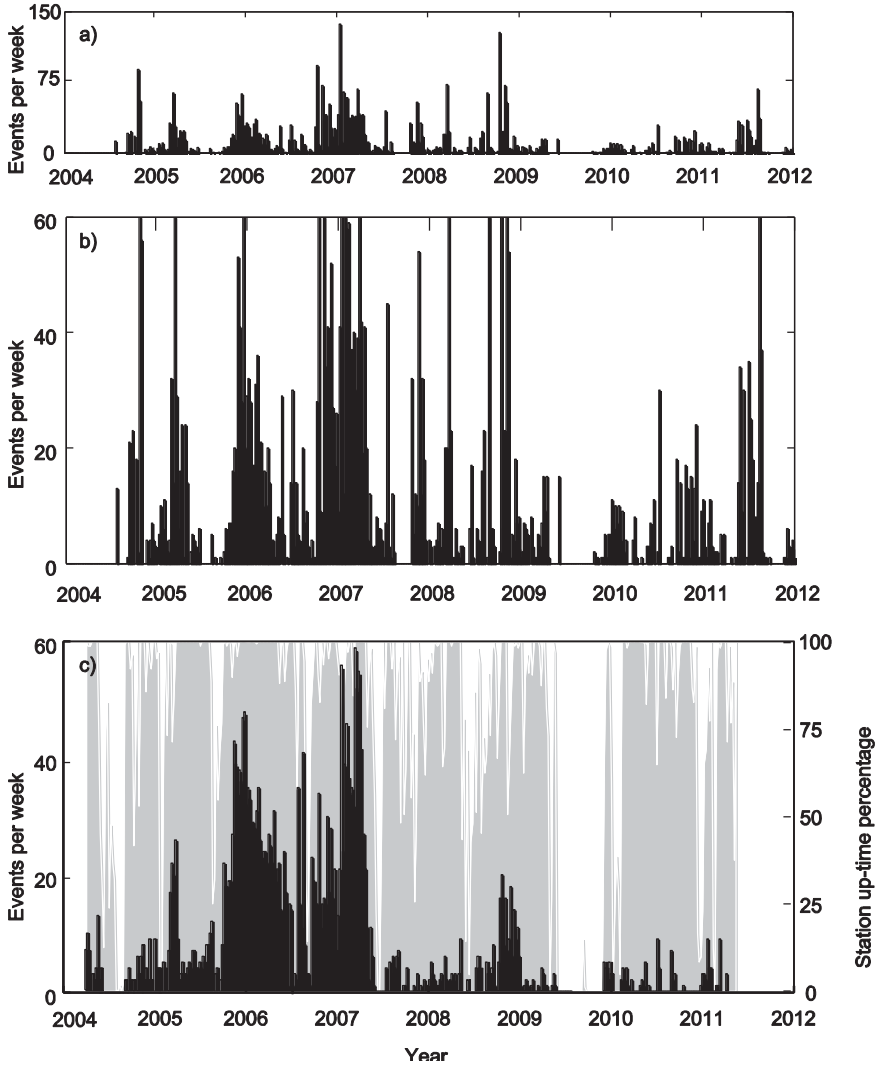

Figure 8

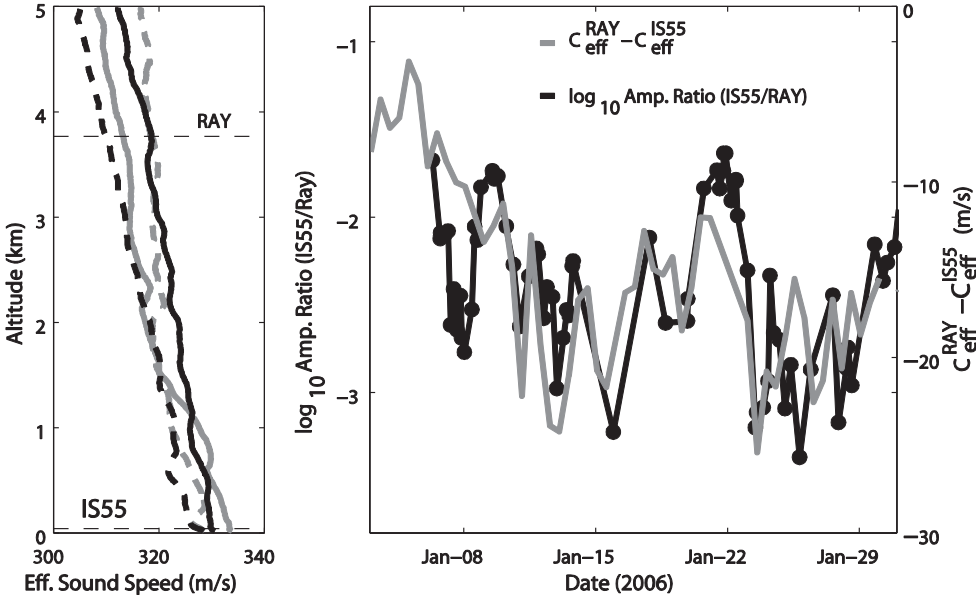

Figure 9

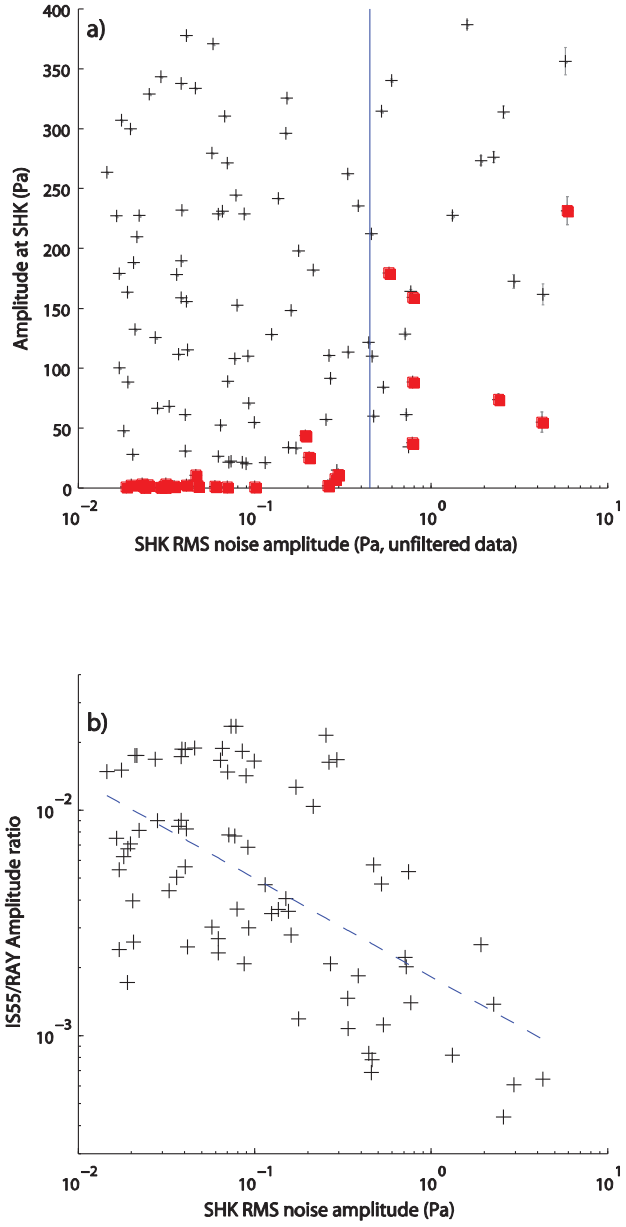

Figure 10

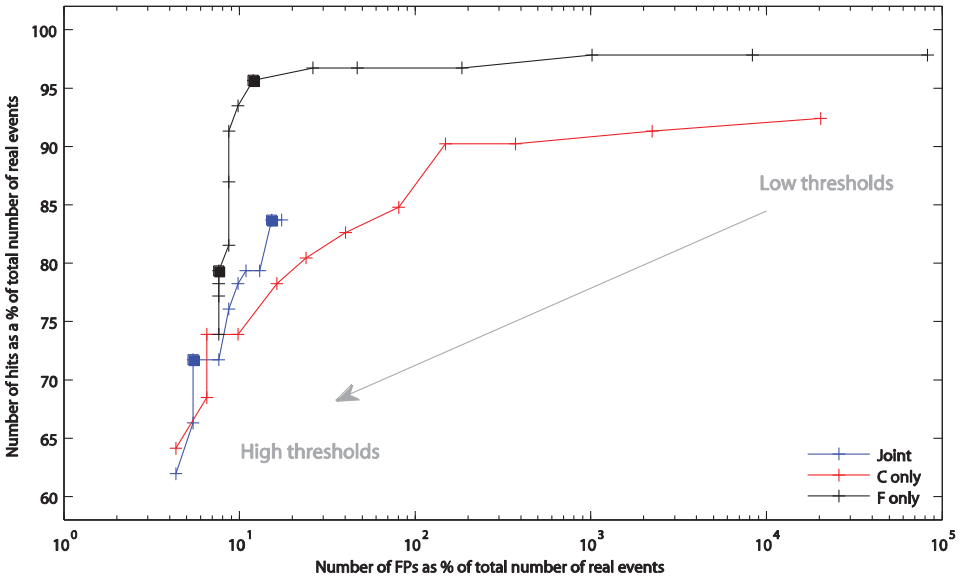

Figure B1

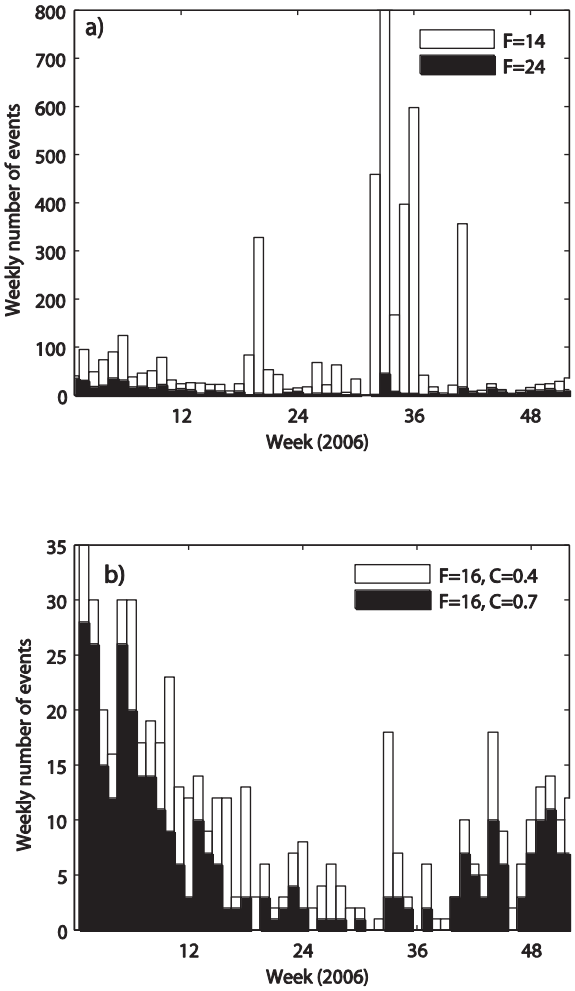

Figure B2

Highlights

A study of volcanic infrasound recorded 25 km from Mount Erebus, Antarctica.

75% of Strombolian events detected at the vent are observed at 25km.

Large amplitude, temporally smooth variation in infrasound amplitude decay with range

Amplitude decay rate depends on lower tropospheric sound speed structure.

Automatic event detection was able to monitor activity levels at Erebus from 25 km.